2017

Measurements of Near Wake Characteristics of a Tidal Turbine under Yaw

Matthew Michael Pasch
Lehigh University

Measurements of Near Wake Characteristics of a Tidal Turbine under Yaw

by

Matthew Michael Pasch

A Thesis

Presented to the Graduate and Research Committee

of Lehigh University

in Candidacy for the Degree of

Master of Science

in

Mechanical Engineering

Lehigh University

August 2017

Approval Sheet

This thesis is accepted and approved in partial fulfillment of the requirements for the Master of Science in Mechanical Engineering.

Measurements of Near Wake Characteristics of a Tidal Turbine under Yaw

Matthew Michael Pasch

_____

Date Approved

_____

Dr. Arindam Banerjee

Thesis Advisor & Associate Professor,

Department of Mechanical Engineering & Mechanics

Lehigh University

_____

Dr. Gary Harlow

Department Chair Person

Department of Mechanical Engineering & Mechanics

Lehigh University

Acknowledgements

I would like to thank my family without who this would not be possible. Lehigh University for providing me with the Presidential Scholarship to continue my studies. Professor Banerjee for giving me the opportunity to do this research, and everyone in the lab for being supportive and helpful every step of the way. I would also like to thank Kanye West for being the soundtrack to my writing.

Table of Contents

List of Tables

List of Figures

1. Abstract

Tidal turbines when subjected to yawed inflow condition exhibit a deficit in performance. In addition to the reduction in the ability of the turbine to capture the kinetic energy of the flow, yawed inflow effects the downstream wake propagation and recovery. Investigation into the downstream wake of a tidal turbine is important for the optimization of the installation of tidal turbine arrays. Experiments were run to capture the velocity profile of the wake of the yawed tidal turbine at various downstream locations including x/R's of 1.0, 2.0 and 4.0. Experiments were run at 0, 5, 10 and 15 degrees of yaw, and at varying radial locations from the rotor of the turbine from a z/R of 0.50 to 1.25. The purpose of this thesis is to characterize the downstream near wake characteristics of a yawed tidal turbine using various parameters, including non-dimensional velocity, swirl number, skewness, kurtosis and turbulence intensity.

2. Introduction

Hydropower comes in many forms, Tidal Stream Turbines (TSTs) is one way to capture the kinetic energy from flowing bodies of water such as streams, rivers, and oceans. Tidal Stream Turbines are capable of harnessing marine hydrokinetic energy in an analogous form to wind turbines. The focus of this paper will be on a horizontal axis turbine model (HAT). The horizontal axis refers to the turbine rotating in a plane perpendicular to the flow, and horizontal to the ground it is mounted on, this design is very typical to a wind turbine. Tidal Stream Turbines differentiate themselves from traditional hydropower in that they can operate at zero head and at velocities as low as 0.5 meters per second [1]. Traditional hydropower involves high velocity; high head flows that typically involve large construction efforts to implement. Traditional hydro is most easily visualized as projects like the Hoover Dams, large scale construction projects. The operability range of Tidal Stream Turbines opens a novel approach to harnessing hydropower, as traditional hydropower within the United States has seen a decrease in new facility growth rate. The recent expansions to the United States traditional hydropower fleet have seen significant growth in unit additions and upgrades, additions to existing non-powered dam sites, and low-impact new stream-reach development [2]. The majority of generation capacity being added to the traditional hydropower fleet is through generation being added to existing non-powered dam (NPDs) sites [2]. The slow growth in new capacity construction of traditional hydropower allows room for less constrained growth in marine hydrokinetic energy, primarily through Tidal Stream Turbines.

Tidal Stream Turbines due to their ability to be installed without a dam or other divisionary structures can be installed closer to load, and lower transmission losses / capital costs. This minimizes the initial costs required for installation, and ensure comparatively quicker construction periods compared to traditional hydropower projects. The differences in the construction and setup

of Tidal Stream Turbines from traditional hydropower allows TSTs to capture energy that cannot be harnessed using traditional hydropower. Although this should not minimize the issues that can arise when constructing a Tidal Stream Turbine project. Environmental and grid availability issues remain stumbling blocks for a widespread adoption of projects of this type [3]. The energy available through hydrokinetic energy extraction in the United States has been estimated to be around 370 TWh per year using currently existing technology. This would represent approximately 10 % of the United States current energy usage. Total theoretical hydrokinetic energy available estimates range from 50 to 90 % of the total energy production of the United States [4].

Historically, the European Union has led with investments in the field of hydrokinetic energy; it is estimated that approximately 50 % of global research and development in hydrokinetic energy is within the EU. Out of the total investment in tidal technology, approximately 76 % of that is in horizontal axis turbines. HAT's represent a high technology readiness devices, as in the United Kingdom since 2008 more than 10,250 MWh of energy has been generated from bottom-mounted horizontal-axis tidal turbines. The technological readiness and growth have brought commercial entities into the field of marine hydrokinetic energy as they develop their own form of extraction devices. While it is estimated that 51 % of tidal companies around the world reside within the EU, there have been high profile projects within the United's States. An example of a high profile project within the United States includes Verdant Power's Roosevelt Tidal Energy Project located on the East River [3].

The energy available for extraction for a horizontal axis turbine is proportional to the area swept by the turbine. Practicality and cost effectiveness dictate that to maximize the power harnessed from tidal turbines, they be installed in arrays, rather than by increasing the size of a singular turbine. The installation of turbines into 'arrays' places a variety of variables into the flow

field. A turbine in the second row of an array of turbines is now in the wake of the first row, which has the possibility to cause significant disturbances to the downstream turbine. Additional consideration concerning the inflow of a tidal turbine is the yaw angle to which the flow is at with respect to the front of the turbine, and the skew angle the wake passes by the tidal turbine at. The ability to both study the wake effects from tidal turbines, as well as quantify the effect on performance is a crucial point of interest for this research.

The effect of yaw angles in the inflow direction on wind turbines has been an area of research within the wind turbine community for a period of quite some time. It appears the effect of yaw on wind turbines were notices as early as 1939 during the initial introduction of some of the first commercial wind turbines in the United States [5]. However, it appears the studies that attempted to quantify the effects of the yawed inflow for wind turbines did not occur until several decades later in the 80's [6]. Previous work has concluded that the power reduction factor due to the effect of yaw for a wind turbine can be approximated by a curve of cosine squared of the yaw angle (γ) [7].

Krogstad and Adaramola studied the near wake effects and changed in the turbine performance due to yaw [8]. The wake was observed to gradually move towards the direction of yaw as well as increasingly become non-uniform as the yaw angle increased. Due to the flow, not being symmetric as it crosses the rotor plane, the wake that is generated is additionally asymmetric. The effect on a downstream turbine's wake can be characterized as being subject to lower velocities, higher average turbulence intensity, and a higher rotational speed compared to the wake of a turbine unaffected by surrounding bodies. Medici shows a clearer focus on the wake effects in general and less on the effects that would be incurred on a downstream turbine. Medici states that a yawed turbine clearly defects it's wake to the side. The effects of the deflected wake are

dependent on both the yaw angle and downstream position [9]. The movement of the downstream wake of a yawed turbine to the side is commonly referred to as the meandering of a turbine's wake.

Additional study has been done on the meandering movement of the wake of a turbine yawed to inflow. Jimenez et al. studied the deflection of wake due to yaw by using LES techniques, by measuring at the various downstream location and determining the midpoint in between locations that are at 95% of the free stream velocity [10]. Studies in a similar fashion have additionally been performed by Parkin et al. and Howland et al., both of which conducted experiments on a non-rotating wind turbine in yaw to study wake deflection [11, 12]. The center of wake has additionally been calculated as the 'center of mass' of velocity deficit at locations downstream from a turbine [13].

There has not been significant experimental work into the effect of yaw on either the performance of wake signature of a tidal turbine. Modali computed CFD simulation of the effects of yaw on both a tidal turbines performance and wake signature, however only was able to draw comparison to experimental calculation pertaining to performance [14]. Galloway performed Blade Element Momentum (BEM) simulations and used cursory experimental work to determine both performance and fluid structure interactions, his research once again shied away from wake analysis [15]. Galloways work focused primarily on performance BEM, and cyclic loading due to waves and misaligned flow calculated through BEM analysis. Park et al. performed fluid structure interaction simulation to look at performance and blade deformation [16].

The focus of this thesis will be to investigate the wake signature of a yawed tidal turbine experimentally. The wake signature of a tidal turbine at various yawed inflow angles will be investigated with an Acoustic Doppler Velocimeter with the intent to determine streamwise velocity profiles at various locations both radially and downstream from the rotor plane. These

experiments will be conducted with the purpose to examine the wake of a yawed tidal turbine and examine how the wake can be characterized. In the Methodology section, the wake effect experiments, the design of the prototype turbine, as well as the characterization parameters used will be discussed.

3. Methodology

3.1. Experimental Methodology: Setup

Water Tunnel

All experiments conducted over the course of this thesis were in a Water Tunnel Facility Model No. 505 (Engineering Laboratory Design, MN U.S.A) here in Packard Laboratory at Lehigh University. The water tunnel in questions has a free surface test section .61 meters wide, .61 meters deep, and is 2 meters long. The maximum flow speed the water tunnel is capable of obtaining is 0.95 meters per second. All the experiments for this project were run at a free stream velocity of 0.73 meters per second.

Turbine & Blade Design

The lab-scale marine hydrokinetic turbine used consists of a horizontal axis turbine driven by an NEME23 stepper motor. The design consists of a stepper motor attached to a coupling, to reduce off axis loading, then attached to the main shaft. The main shaft runs through two copper bearings within the nose cone before the rotor is placed onto the end of the shaft. Attached to the back end of the stepper motor is a Futek multi-axis sensor capable of sensing both thrust and torque. The nose cone, body, and end cap are made from an acrylic plastic. The base of the shaft where the mounting post is attached to the body of the turbine assembly is made from stainless steel. The main rotating shaft and rotor are made from an aluminum alloy. Using the stepper motor, it is possible to accurately set the angular velocity of the rotor of the turbine.

The rotor used for this experiment consists of the SG 6043 hydrofoil profile with zero twist. The rotor has a radius of R = 0.14 m and a constant cord length of c = 0.01767 m. The turbine blades are held together inside the hub, so the pitch angle can be set and adjusted. For all

experiments, the pitch angle was kept constant at a pitch angle ($\theta_p = 10^o$) of 10 degrees. Below are CAD file images, as well as photographs of the turbines setup and design. The CAD images have screws, and through-rods omitted to make the design clearer for the viewer, while the final prototype design does not.

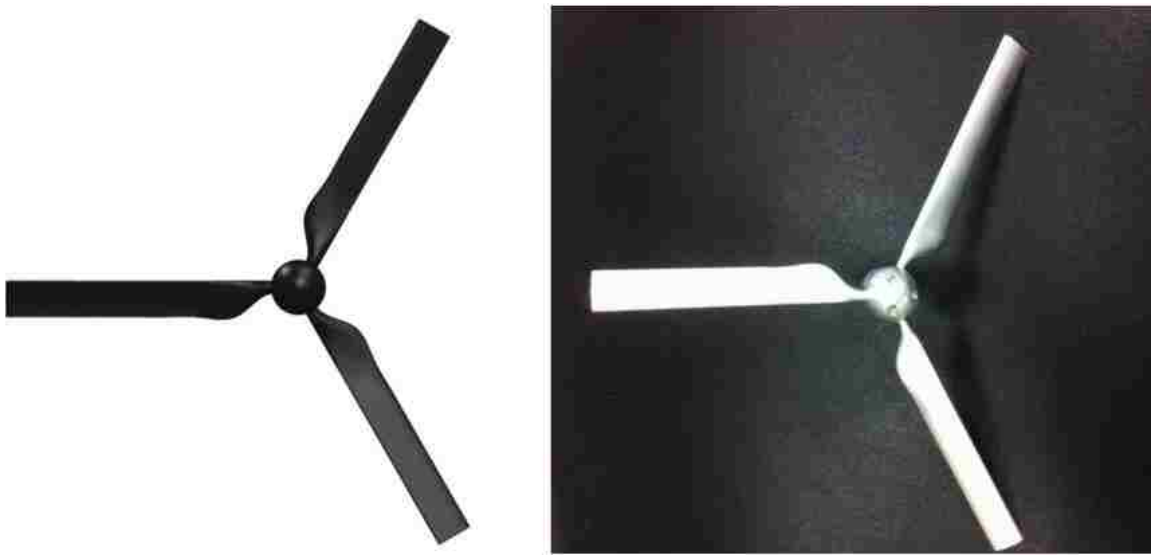

Figure 1: CAD Model (left) and Physical Turbine Rotor (right) [17]

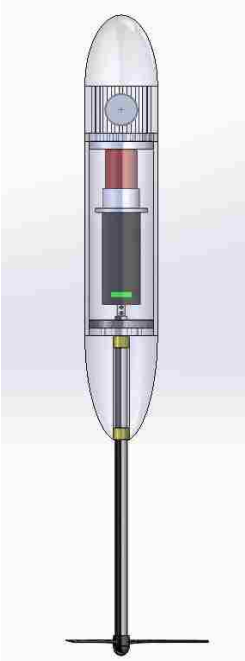

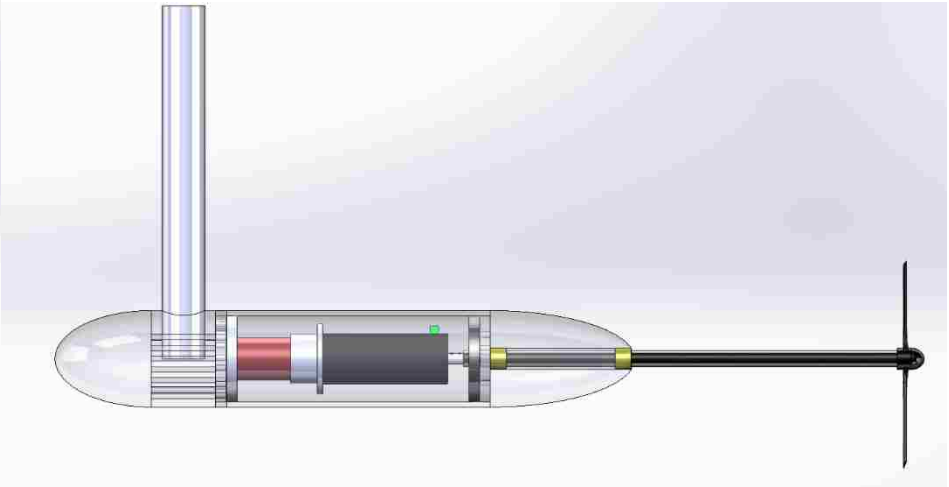

Figure 2: Top View Model Turbine CAD & Figure 3: Side View Model Turbine CAD

Figure 4: Side View Model Turbine Prototype & Figure 5: Top Down View Model Turbine Prototype

As can be seen in Figure 5: Top Down View Model Turbine Prototype the square bracket on the top of the setup holds the turbine steady in the streamwise direction while allowing the shaft to rotate. The circular plate above the square bracket can be fixed not to allow the turbine to rotate so that the overall turbine can be set at certain yaw angles (γ) to the inflow. The placement of the turbine within the tank can traverse in a crosswise direction to correct for wall effects around the rotor. During each experimental run, the crosswise placement of the turbine body was adjusted so that the rotor remained in the center of the test section.

The sensor when in steady state operation can measure the torque that the hydrofoil rotor is imparting onto the shaft to determine the power coefficient of the turbine at that operating point. The power coefficient is determined by measuring the torque (T) imparted onto the rotating shaft of the turbine, as well as the angular velocity (ω) of the rotating shaft. The denominator is the power available for extraction within the flow where U_∞ is the free stream velocity, and A is the area swept by the rotor. This value is calculated from the experimental results through Equation 1 and can be compared to simulations, whether those simulations are computational fluid dynamics, or based on blade element momentum theory.

$$C_P = \frac{T\omega}{\frac{1}{2}\rho A U_\infty^3} \tag{1}$$

3.2. Wake Methodology using an Acoustic Doppler Velocimeter (ADV)

The wake of the prototype turbine was measured using a Vectrino Acoustic Doppler Velocimeter (ADV). The ADV device is used to measure 3D water velocities at a specific point in space. The data output of the ADV device is a time series of the velocity components (< *u(t), v(t), w(t)* >) at the specific point in space you are measuring. The accuracy of the device used is ± 1%

of measured value or 1 millimeter per second. The sampling volume for this experiment consists of a 6-mm diameter sphere, 50 mm below the top of the probe. The Echo intensity of the probe operates at 10 MHz on a linear scale with a 25 dB (decibel) range. The ADV additionally consists of a thermistor embedded in the probe that has an accuracy of 1 degree Celsius to correct for a temperature change in the working fluid.

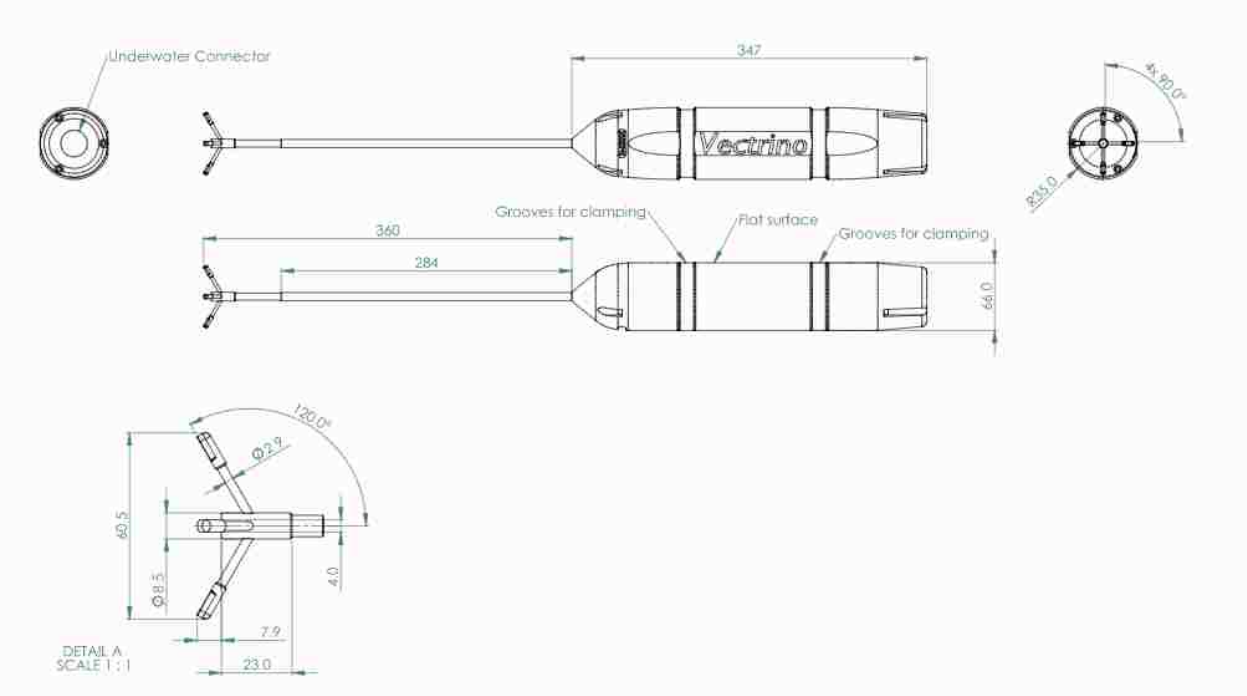

Figure 6: Vectrino 2D-3D Down Looking, fixed stem product drawing [18]

An ADV works by sending out an acoustic signal in three dimensions. The acoustic wave sent out from the transmitter is sent at a fixed frequency. That acoustic wave then bounces back to the dual receivers that are aligned in *u* (streamwise) and *v* (crosswise) directions respectively. The receiving nodes record the frequency of the signal that is bounced back off the moving particulate matter in the water. Based on the Doppler shift in returning frequencies to the ADV, the components of the flow velocities in the sampling volume is then calculated. The return

frequencies are adjusted for the speed of sound in the liquid medium the test is being run in, this is determined from the temperature measurement that occurs within the probe. The below formula is used for the calculation, where *V* is the unknown velocity component (*u, v, w*), *c* is the speed of sound in water at the time of measurement, and *f* is the received and transmitted frequency respectively.

$$f_{recieve} = f_{transmit}\frac{V}{c} \tag{2}$$

The model ADV used in this experiments consists of two sets of probes each capable of sensing both their main orientation and an orientation of velocity perpendicular to their main orientation. In this case, the results of the ADV consists of *u*, *v* and two *w* measurements. Each *w* measurement is based off either *u* or *v* set of probes on the ADV. In this paper the *w* (vertical) velocity component is negligible in all calculations it is used in.

Due to experimental constraints, the ADV will be used at various *x* distances downstream of the rotor for the top half of the wake. No measurements are made that consist of velocity points below the rotating shaft of the turbine, this is due to the constraints of the physical apparatus. An array of points will be taken in both the *y* and *z* directions to cover the full threshold of the turbine's wake profile. The downstream effects will be studied to observe how changes in yaw angle affect wake propagation. Below is a diagram of the experimental setup that includes a simplified experimental data point layout.

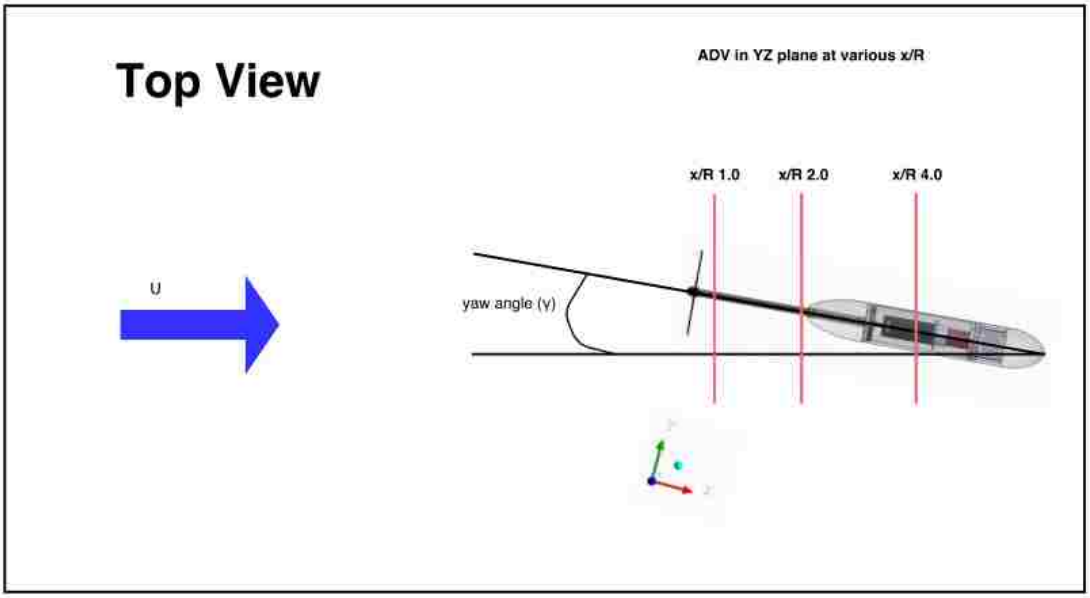

Figure 7: Top Down View of Experimental Setup

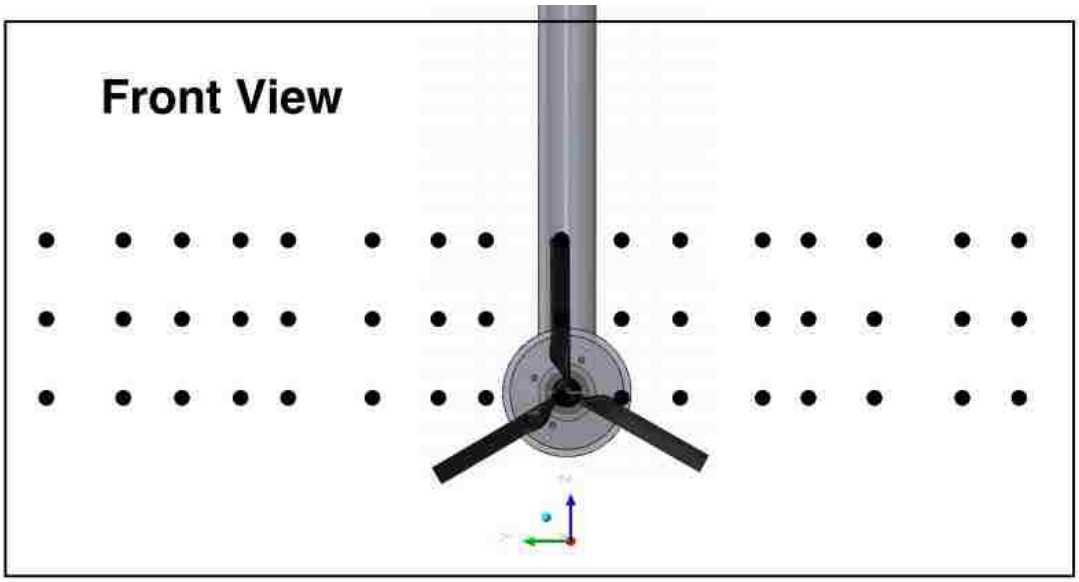

Figure 8: Front View of Wake Experimental Setup[1]

[1] Black dots represent data points. Some data points are omitted for a better view of setup.

3.3. Experimental Parameter Calculations

By capturing the velocity vector components at each experimental data point, the velocity profile can be plotted for various cases of the operation of the turbine. This allows us to observe the velocity deficit in the wake as well as observe the downstream propagations of the wake. At each data point the average velocity, turbulence intensity, skewness and kurtosis of the flow can be calculated.

Figure 9: Side View Model Turbine in Water Tank with ADV Probe

From each time trace provided by the ADV the mean ($\overline{V}$), standard deviation (σ), skewness (s) and kurtosis (k) is calculated for each point. The non-dimensional velocity is used for data reporting is reported as V^* for cases shown below. Post processing is completed in MATLAB using the below

formulations for calculation, where *V* is a stand-in for any individual component of the velocity vector.

$$\bar{V} = \frac{1}{N}\sum_{i=1}^{N} V_i \tag{3}$$

$$V^* = \frac{\bar{V}}{V_\infty} \tag{4}$$

$$\sigma_V = \left[\frac{1}{N-1}\sum_{i=1}^{N} |V_i - \bar{V}|^2\right]^{\frac{1}{2}} \tag{5}$$

$$s_V = \frac{\left[\frac{1}{N}\sum_{i=1}^{N}(V_i - \bar{V})^3\right]}{\left(\left[\frac{1}{N}\sum_{i=1}^{N}(V_i - \bar{V})^3\right]^{\frac{1}{2}}\right)^3} \tag{6}$$

$$k_V = \frac{\left[\frac{1}{N}\sum_{i=1}^{N}(V_i - \bar{V})^4\right]}{\left[\frac{1}{N}\sum_{i=1}^{N}(V_i - \bar{V})^2\right]^2} \tag{7}$$

Using the average velocity at each point is it possible to calculate the velocity wake profile at various locations of the flow. The standard deviation allows the calculation of the Turbulence Intensity, the meaning of this is expounded upon below. Skewness is a measurement of the asymmetry of the data, and kurtosis is a measurement of how outlier prone a distribution is. Each

of these variables is used to characterize the wake propagation of this flow at various downstream and radial locations in the flow.

Turbulence Intensity is a measure of the rate at which energy is transferred from the mean flow to the turbulent eddies that define a turbulent flow. The turbulence intensity (*I*) of flow is one of the most common parameters used to define the turbulence of flow in marine energy applications. The physical significance of turbulence intensity is that low values represent better aerodynamic properties for the operation of a turbine. The Turbulence Intensity was calculated using the experimental standard deviations, however, in our case, we used the U_∞ and v_∞ values for calculations.

$$I_{2D}^{\infty} = \frac{\frac{1}{2} * [\sigma_u^2 + \sigma_v^2]}{[U_\infty^2 + v_\infty^2]} * 100\% \quad (8)$$

An additional set of experiments were additionally undertaken to identify the swirl number at various degrees of yaw. Swirl number experimentation requires a vertical array of experimental points is taken from the rotor to the tip of the turbine blade. Pictured below is the experimental setup for swirl experimentation.

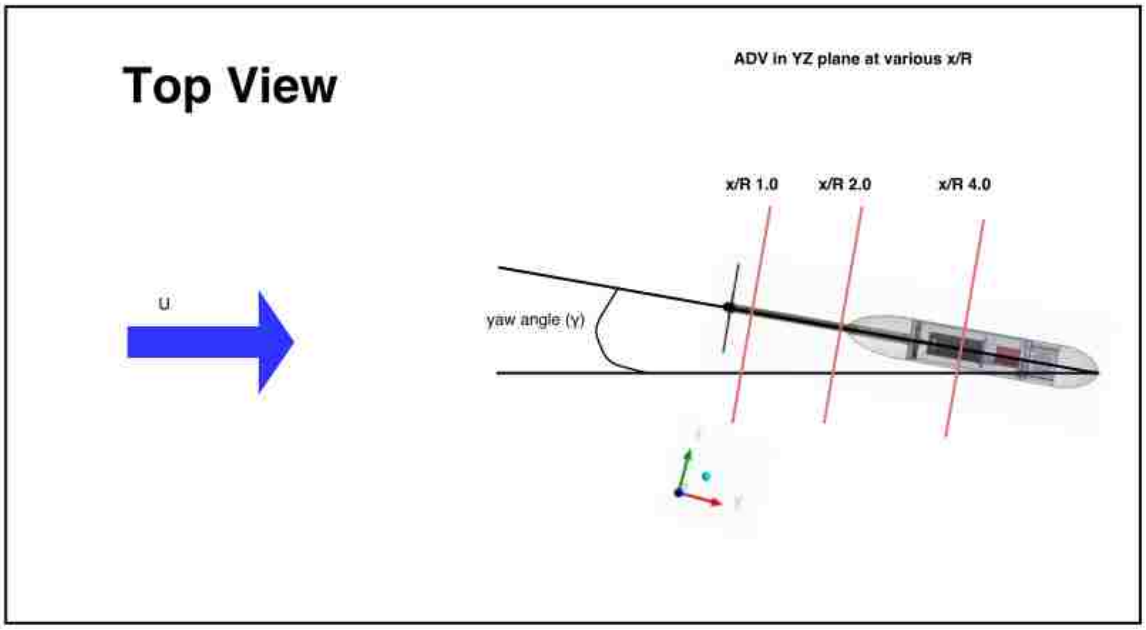

Figure 10: Top Down View Swirl Experimental Setup

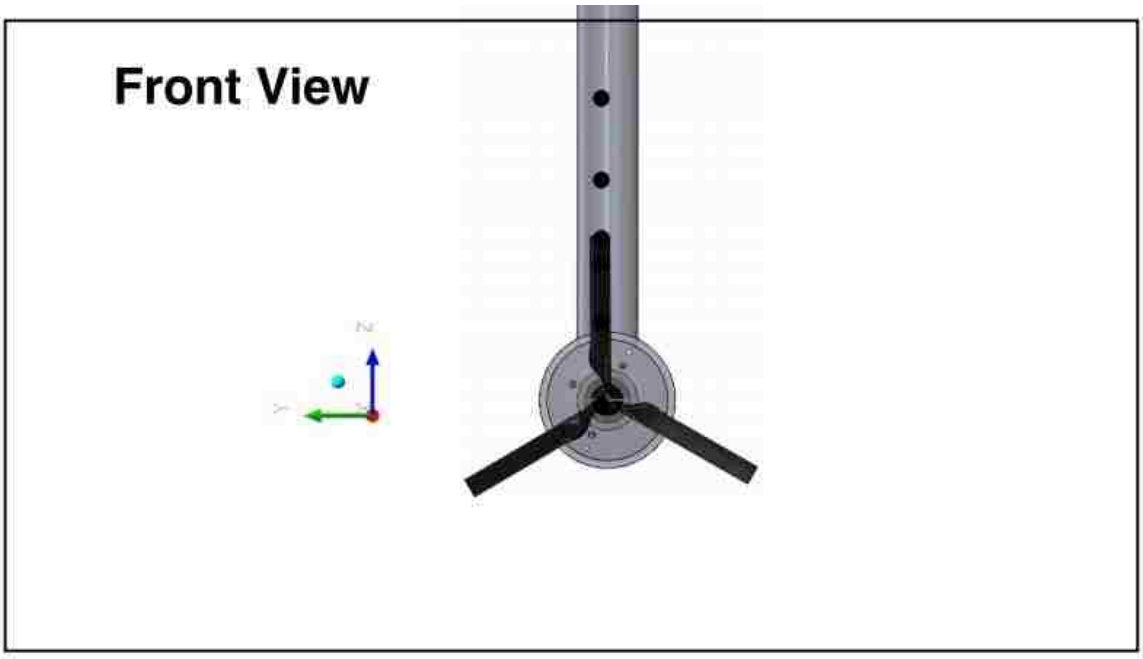

Figure 11: Front View Swirl Experimental Setup[2]

[2] Black dots represent data points. Some data points are omitted for a better view of setup.

The swirl number (S) is calculated as the ratio between the axial flux of angular momentum (G_ϕ) and the axial flux of linear momentum (G_x), where R is the radius of the turbine.

$$S = \frac{G_\phi}{G_x R} \tag{9}$$

Where the fluxes of angular and liner momentum are defined respectively as such.

$$G_{phi} = \int_0^R (vr)\rho r u 2\pi r dr \tag{10}$$

$$G_x = \int_0^R u\rho u 2\pi r dr \tag{11}$$

In the above equations: u is inflow velocity, v is the cross-stream velocity, ρ is the density of water, and r represents distance along the rotor blade. The swirl number is calculated by numeric integration of the momentum fluxes using a trapezoidal approximation. The swirl number is used to define the level of the swirl of the flow, where $S \leq 0.2$ is considered a weak swirl, $0.2 < S \leq 0.5$ is a medium swirl, and $S > 0.5$ is a strong swirl. By calculating the swirl number at various distances downstream of the blade rotor the recovery of the wake can be observed and characterized [19].

Experimental Parameters

The experimental parameters that in this experiment primarily consist of the rotational velocity of the rotor (ω), free stream velocity (U_∞), and yaw angle (γ). For the set of wake experiments that were run both the rotational velocity (ω) and the free stream velocity (U_∞) were kept constant. The yaw angle (γ) was varied from 0 to 15 degrees in increments of 5 degrees. This allows the experimental results to be compared to the previous simulation completed by this lab [20]. Using the ADV the time trace of velocity components (u, v, w) at each experimental point will be measured. TSR represents the tip speed ratio of the blade and is calculated using the below formula,

where U_∞ is free to stream velocity at infinity, R is the rotors blade radius, and ω is the rotational velocity of the rotor.

$$TSR = \frac{U_\infty R}{\omega} \tag{12}$$

Wake experiments are run at the below conditions.

Parameter	Range
U_∞	0.73 m/s
v_∞	0.00 m/s
ω	250 RPM
TSR	5
γ	0, 5, 10, and 15 degrees

Table 1: Experimental Wake Parameters

The conditions above represent the peak C_p the turbine performance. Since in real world operating conditions a turbine will almost always be operating at max C_p tests were run at this operating point to isolate the effect that yaw has on the wake and performance of the tidal turbine.

Experimental data was then taken at each of the below listed locations.

x/R / z/R	1.0	2.0	4.0
0.50	**0,5,10,15**	**0,5,10,15**	**0,5,10,15**
0.75	**0,5,10,15**	**0,5,10,15**	**0,5,10,15**
0.90		**0,5,10,15**	**0,5,10,15**
1.00	**0,5,10,15**	**0,5,10,15**	**0,5,10,15**
1.10		**0,5,10,15**	**0,5,10,15**
1.25		**0,5,10,15**	**0,5,10,15**

Table 2: Wake Results Table[3]

Swirl experiments were run at the below conditions.

[3] Table is populated with the yaw angles recorded, full y/R test section range was recorded for each test case.

Parameter	Range
U_∞	0.73 meters per second
v_∞	0.00 m/s
ω	25 - 250 RPM
TSR	0.5-7.0
γ	0, 5, 10, and 15 degrees

Table 3: Experimental Swirl Parameters

Experimental data was then taken at each of the below listed locations.

x/R / TSR	1.0	2.0	z/R
0.5	0	0, 5, 10, 15	0.13
1.0			0.23
1.5			0.32
2.0			0.41
2.5			0.51
3.0			0.60
3.5			0.69
4.0			0.79
4.5			0.88
5.0			0.97
5.5			1.00
6.0			
6.5			
7.0			

Table 4: Swirl Results Table[4]

[4] Table is populated with yaw angles. Points were taken at the references z/R values.

4. Results: Mean Flow Characteristics

4.1. Mean Velocity

Effect of Yaw Angle

The below plots consist of u^* plotted across the width of the water tunnel (y/R). The turbine is yawed in 5 degree increments in the positive direction. In all experimentation, the rotor remains in the center of the tunnel. These results are taken at an x/R of 1.0 and 2.0 respectively and a z/R of 0.75.

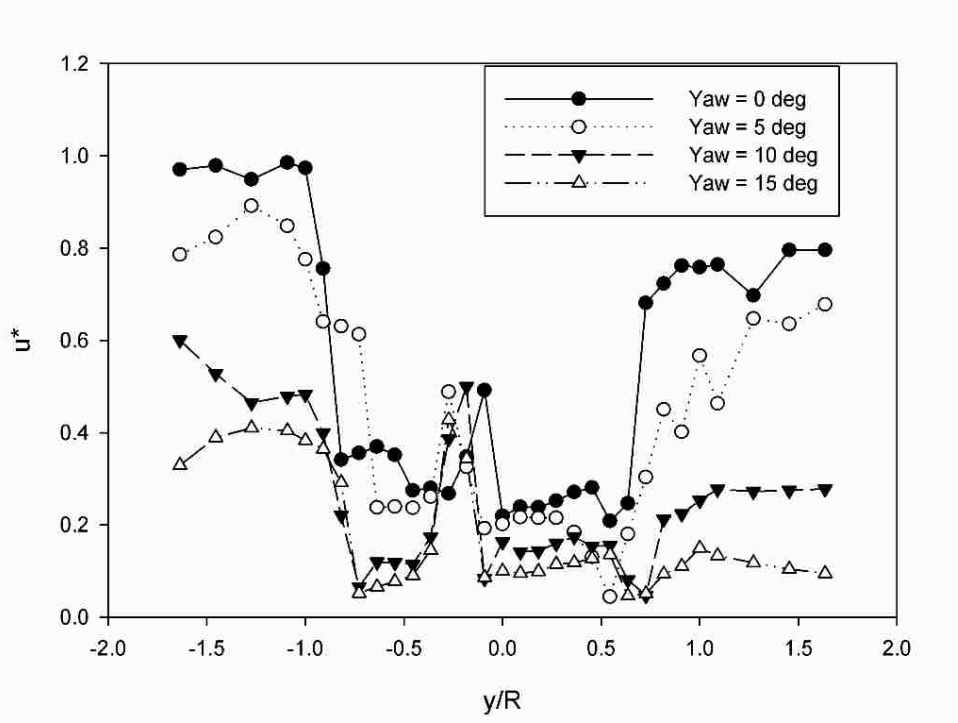

Figure 12: u^* at x/R = 1.0, z/R = 0.75

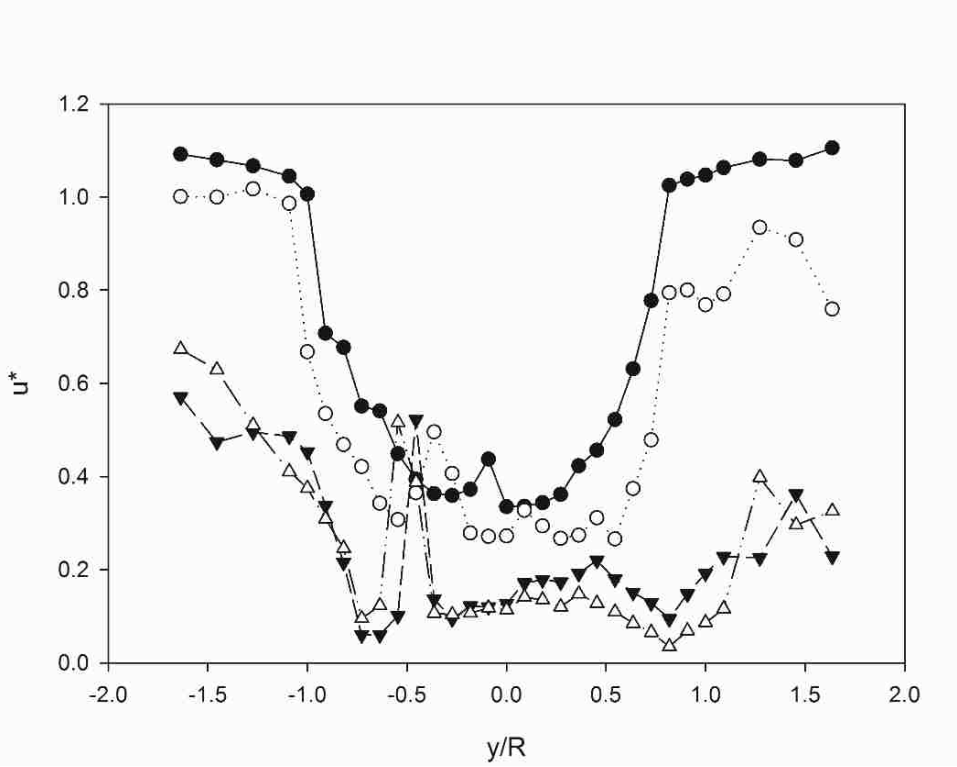

Figure 13: u^* at x/R = 2.0, z/R = 0.75

As it can be seen at an x/R of 1.0 for the baseline 0-degree yaw case, the symmetry that is expected to be seen from the flow has not yet fully developed. It is believed this is due to a requirement for a larger distance to be traveled downstream from the rotor plane until the wake has fully formed. At an x/R of 2.0, the 0-degree yaw case is largely symmetric, as would be expected.

As the yaw angles increase the wake deficit can be seen increasing on the positive side of the flow. As the flow grows farther away from the center of the turbine, the wake begins to recover. The recovery period increases as the yaw angles increases. At higher yaw angles the recovery length is not short enough to be captured in this experimental setup. The increase in velocity deficit

can be seen to increase exponentially from the 0 to 5-degree yaw case, but the 10 and 15-degree yaw case the drop off is much less pronounced.

The spike in velocity seen around the center of the profile is theorized to be from fluctuation from the center of the turbine due to the rotating shaft. These fluctuations are a result of being directly behind the rotor and directly above the rotating shaft. It is observed that with both increasing yaw angle and increasing downstream distance the spike shifts to the negative side of the profile. At an *x/R* of 2.0, the spikes can be observed to increase in magnitude with increasing yaw angle. At an *x/R* of 1.0, the spikes maintain a consistent magnitude regardless of yaw angle.

Characterization at Different Radial Locations

The below plots illustrate the change in *u** versus *y/R* at varying *z/R* heights of the wake profile of the turbine. All results are recorded at an *x/R* of 2.0 behind the turbine rotor.

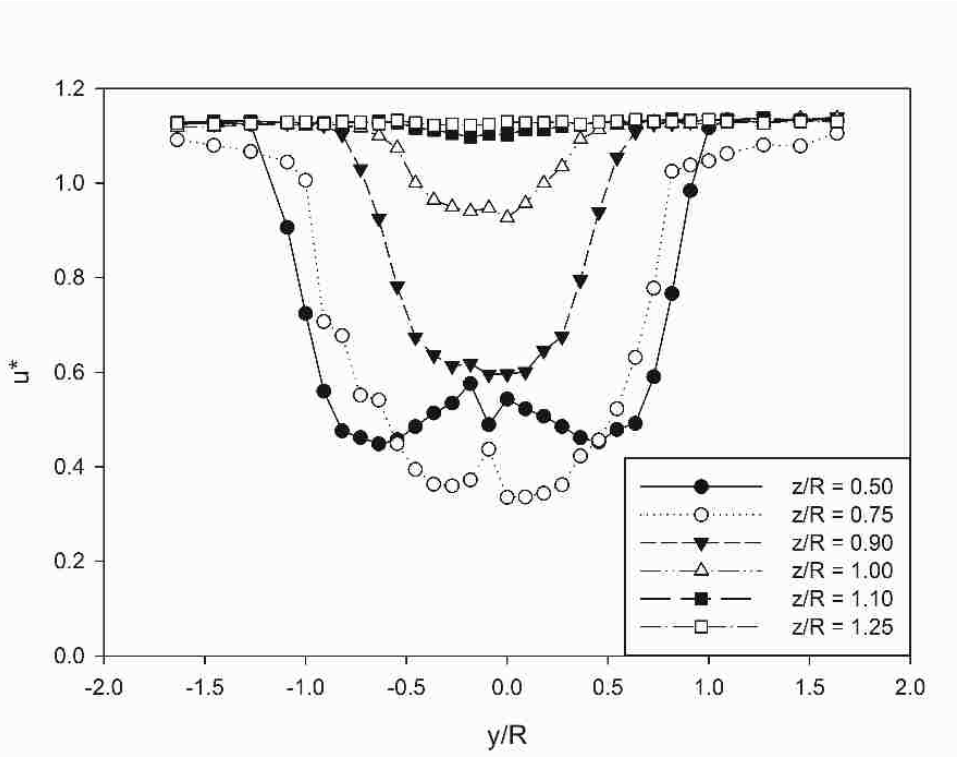

Figure 14: *u** at *x/R* 2.0, Yaw 0 deg.

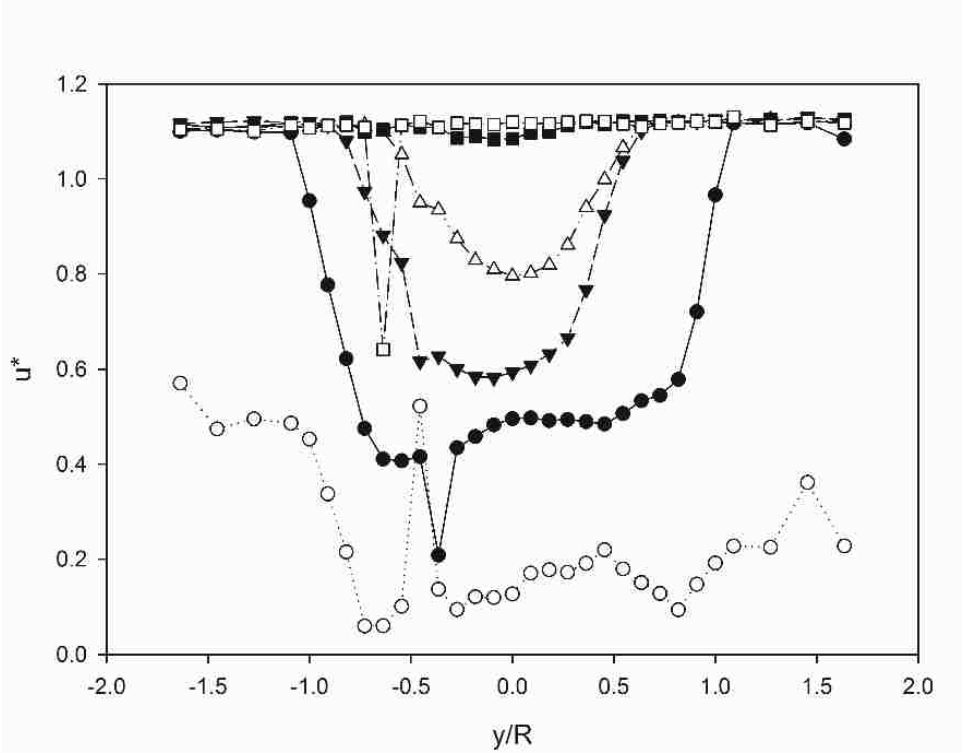

Figure 15: *u** at *x/R* 2.0, Yaw 10 deg.

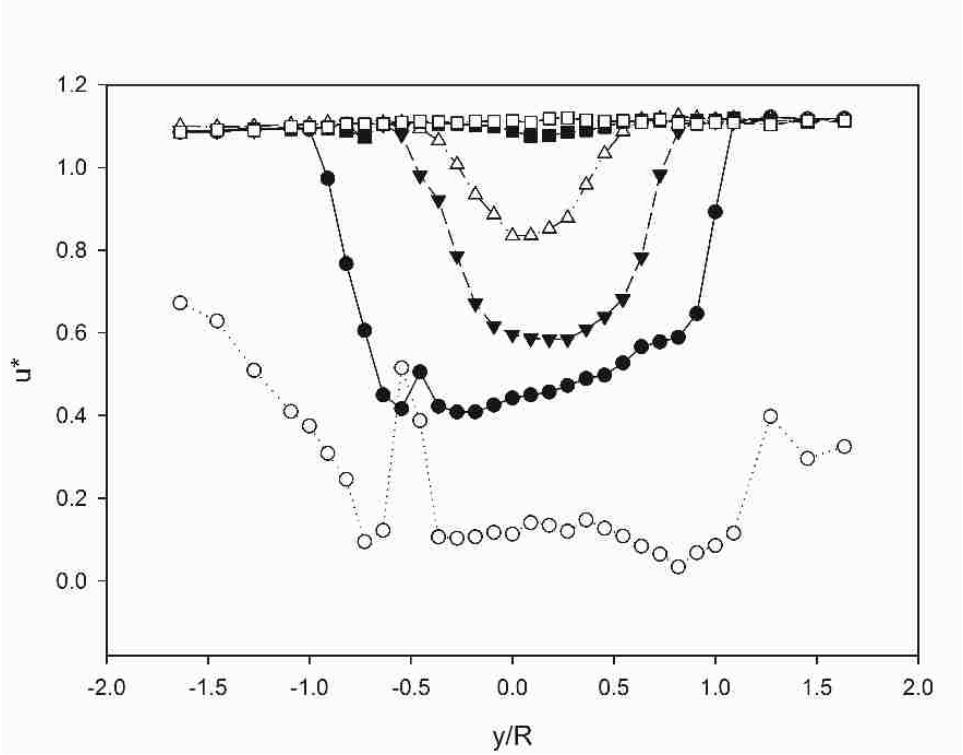

Figure 16: *u** at *x/R* 2.0, Yaw 15 deg.

As it can be observed as the yaw angle increases the velocity deficit recovery on the side of the yawed turbine suffers as the yaw angle increases. At an *x/R* of 2.0, this effect is most pronounced, an *x/R* of 1.0 does not allow the wake to form fully and farther distances back are prohibitive due to the experimental setup.

In the 0-degree yaw case, a symmetric wake is evidenced. There is a velocity deficit in the immediate wake of the rotor. This velocity deficit is a show to recover quicker as the height above the rotor is increased. The velocity deficit is additionally less pronounced as the height above the rotor is increased. At a *z/R* of 1.10, the velocity of the flow is approximately flat depending on location. The velocity at a *z/R* of 1.10 and 1.25 approximately match what would be the bypass velocity of the turbine. This would evidence that we are observing the top of the wake. However, we are not yet far enough away from the turbine to be beyond the bypass region where we see an increased velocity greater than the free stream U_∞ of 0.73 meters per second. The free stream velocity would be shown by *u** of 1.0 in the above plots.

The spread of the wake can be observed to increase as the yaw angle increases. The velocity deficit proceeds to spread out as the yaw angle increases. The 0-degree yaw case exhibits a symmetric wake profile. However, as the yaw angle increases the velocity profiles radially in the middle of the wake appear to spread out as the recovery of the deficit slows. This can be shown by the increase in the skewness of the velocity profiles. As you progress radially up, there is no longer a large difference in skewness. At radial distances of *z/R* of 0.50 and 0.75, the increase in skewness can be observed with an increase in yaw angle. This indicates a spreading of the wake across the full cross section of the water tunnel.

z/R / Yaw	0.50	0.75	0.90
0 deg.	0.70	0.18	-0.60
10 deg.	0.51	1.04	-0.58
15 deg.	0.51	1.12	-0.65

Table 5: Skewness Comparison at Various Yaw and Radial Locations.

Characterization at Different Downstream Locations

The below plots illustrate the change in *u** versus *y/R* at varying yaw angles and at varying downstream locations.

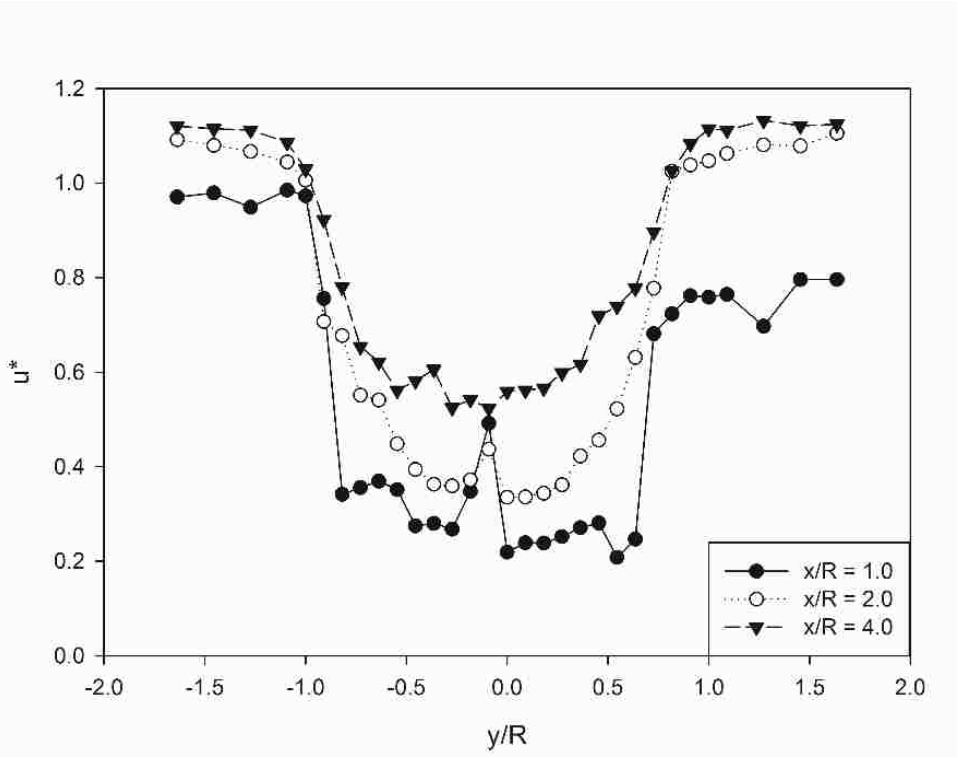

Figure 17: *u** at *z/R* 0.75, Yaw 0 deg.

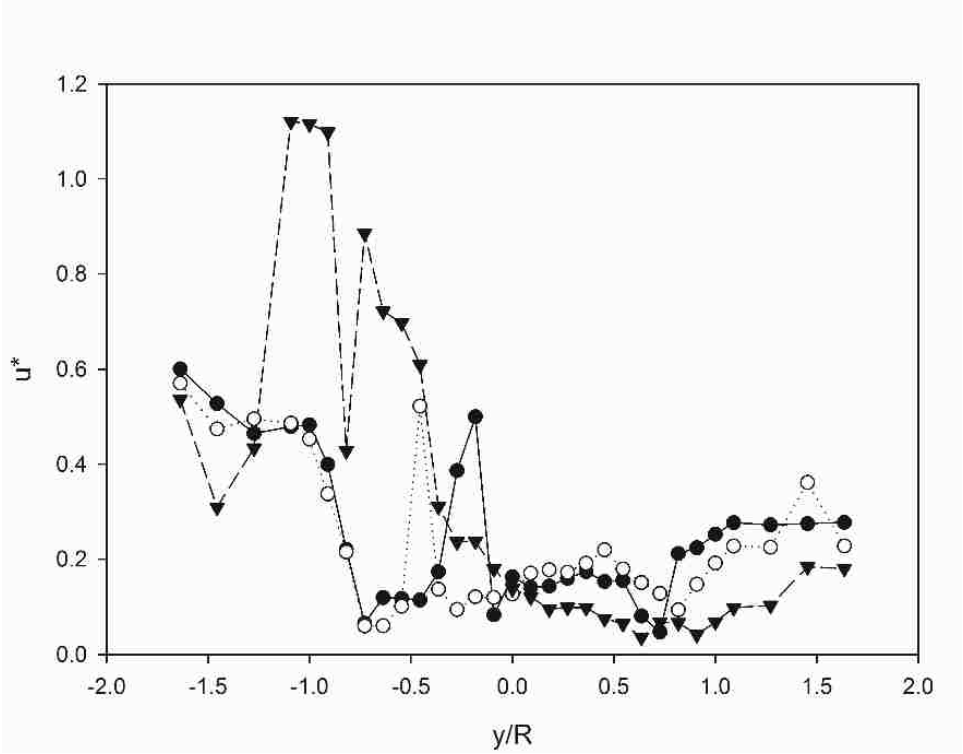

Figure 18: *u** at *z/R* 0.75, Yaw 10 deg.

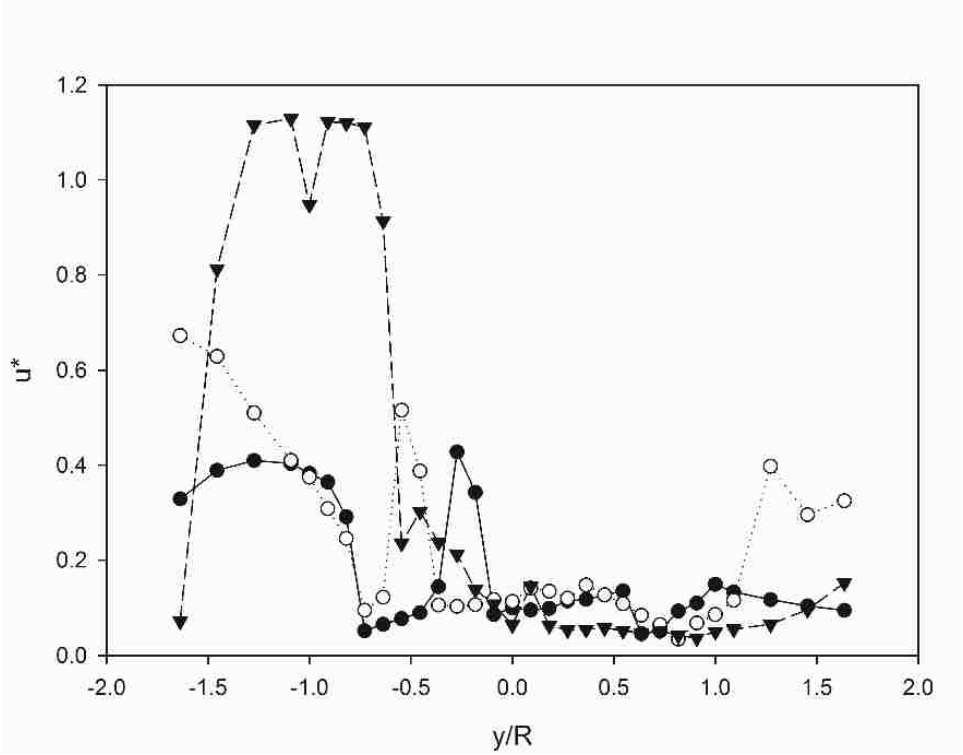

Figure 19: *u** at *z/R* 0.75, Yaw 15 deg.

In the 0-degree yaw case, the velocity profile of the wake remains symmetric as the downstream distance from the rotor increases. As the downstream distance increases in the 0-degree yaw case, the velocity deficit was seen in the center of the velocity profile decreases and recovers as the wake progresses downstream.

As the yaw angle increases, there is no noticeable change in the ability of the wake to recover as the downstream location increases. It is possible that this is a result of the radial position. A radial position of z/R equal to 0.75 is where the most pronounced variation in flow is observed. Thus it would be possible that observations at a different radial location would result in a more noticeable trend.

What is of note from these plots is that the negative side of the velocity profile proceeds to recover much faster as the yaw angle increases. The negative portion of the velocity profile at an x/R of 4.0 at a high yaw angle nears the same profile of that of the 0-degree yaw case. It can additionally be noticed that as this profile approaches the near wall region, the velocity proceeds to drop in magnitude. It is unclear if this recovery is due to the downstream distance or due to another effect. It is theorized that the drop-in magnitude as the profile approaches the side walls of the water tunnel is due to wall effects and approaching the body of the turbine. When observing the velocity profile at a downstream distance of x/R equal to 4.0 the sensor is observing above the body of the turbine as opposed to the other downstream distances where it is above the shaft. It is possible that the effects due to the body could throw off some of the results.

4.2. Turbulence Intensity

Effect of Yaw Angle

The below plots illustrate the change in the turbulence intensity profiles at a constant *x/ R*, *z/R* and with a varying yaw angle.

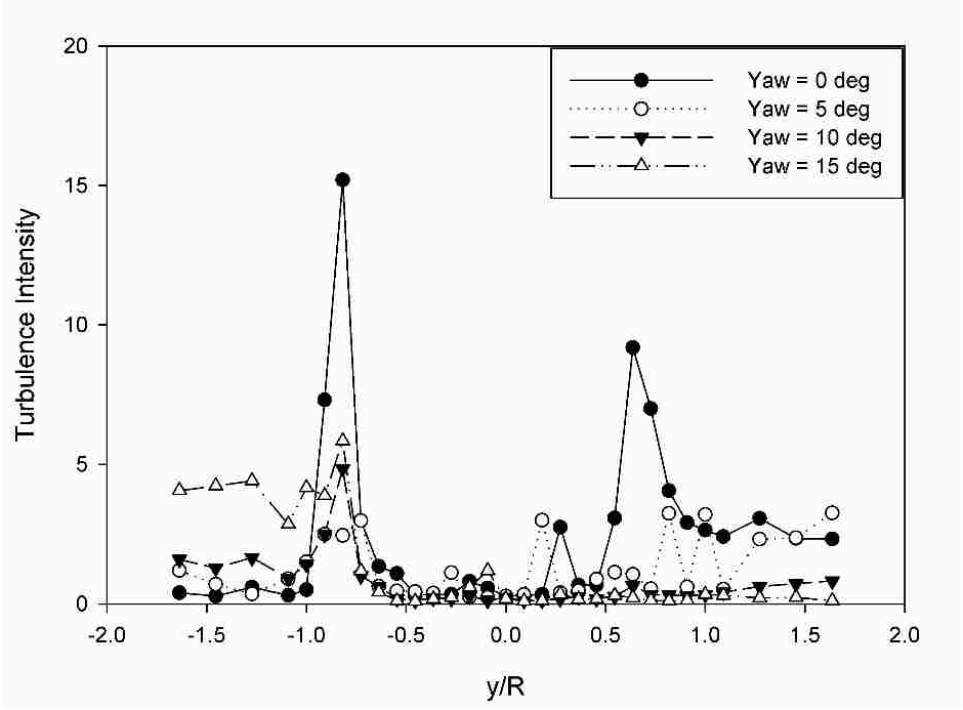

Figure 20: Turbulence Intensity at x/R = 1.0, z/R = 0.75

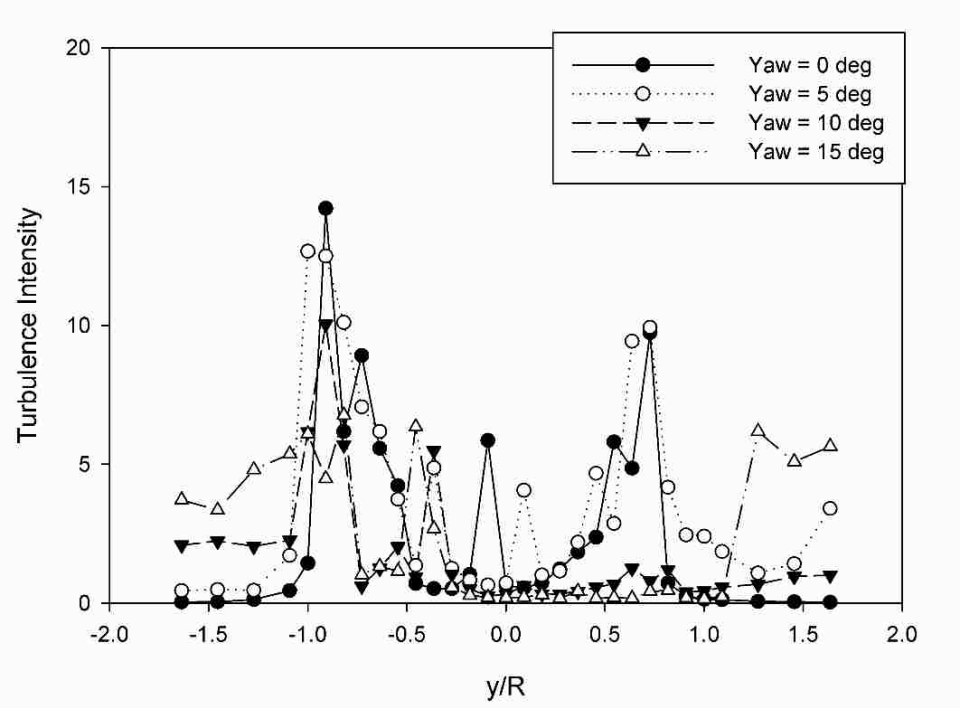

Figure 21: Turbulence Intensity at x/R = 2.0, z/R = 0.75

The Turbulence Intensity spikes at both an x/R of 1.0 and 2.0 at approximately the radial locations of the tips of the turbine rotor. This would represent the capturing of the tip vortices being shed from the turbine blades. The overall magnitude of the turbulence intensities tends to increase once the downstream distance is moved from 1.0 to 2.0 radiuses back from the turbine. As it is expected to be seen, there is generally a low level of turbulence intensity at regions of the wake profile that are not centered on an area of interest, the center of the rotor or the tips of the blades.

At an x/R of 1.0, no clear trend portrays itself with the increase in a yaw angle. It appears that at a yaw angle of 0 the largest turbulence intensity spikes are seen, presumably from the tip vortices of the rotor. As the yaw angle increase these spikes in turbulence intensity are no longer seen. This is possible a result of experimentation where the tip vortices are traversing in a vertical

direction, and they are not captured at a *z/R* of 0.75. There is an observable trend on the positive side of the wake beyond *y/R* of 1.0. The turbulence intensity levels tend to increase with increasing yaw angle beyond the rotor tips as the wake approaches the wall of the water tunnel. This trend does not appear to represent itself on the negative side of the profile in the *y/R* of -1.0 and beyond the region.

At an *x/R* of 2.0, there is larger magnitude turbulence intensities than at an *x/R* of 1.0. Spikes on the negative side of the velocity profile are consistent with a *y/R* of 1.0 regardless of yaw angle. On the positive side of the velocity profile turbulence intensity spikes are only present at a *y/R* of 1.0 for the smaller yaw angles of 0 and 5 degrees. Beyond the range of one rotor radius for both sides of the wake profile, there is a noticeable turbulence intensity background. This back ground is at an increased level than the *x/R* 1.0 profile. The turbulence intensities in this region appear to increase with increasing yaw angle. This would seem to signal that by increasing the yaw angle coincides with increases in the background turbulence intensity of the flow.

Characterization at Different Radial Locations

The below plots illustrate the change in turbulence intensity for varying radial *z/R* depths for one yaw angle and downstream distance.

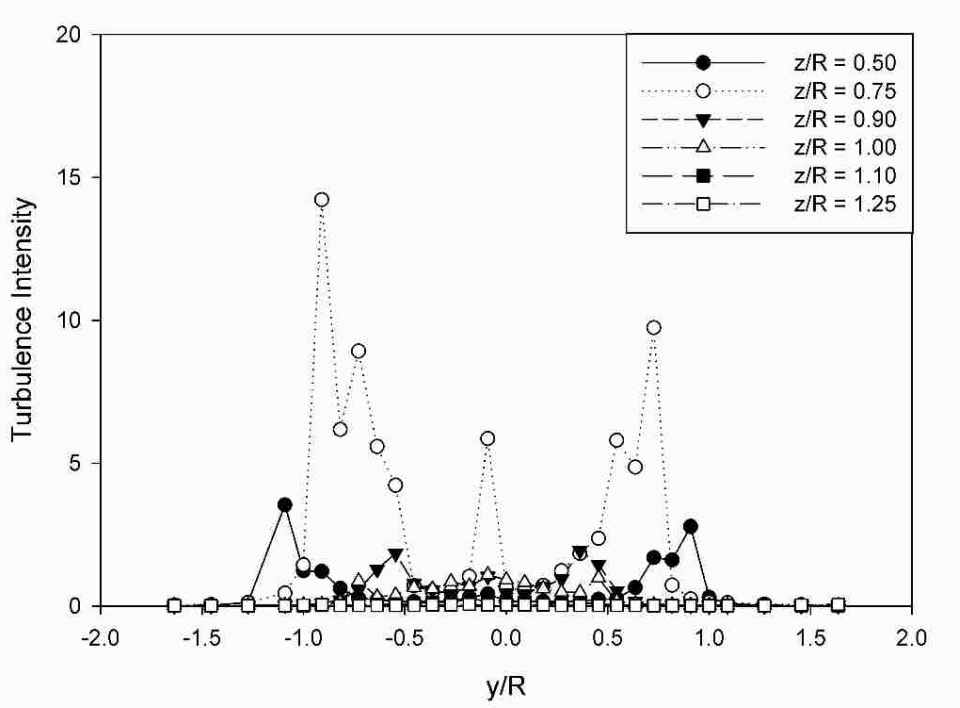

Figure 22: Turbulence Intensity at *x/R* 2.0, Yaw 0 deg.

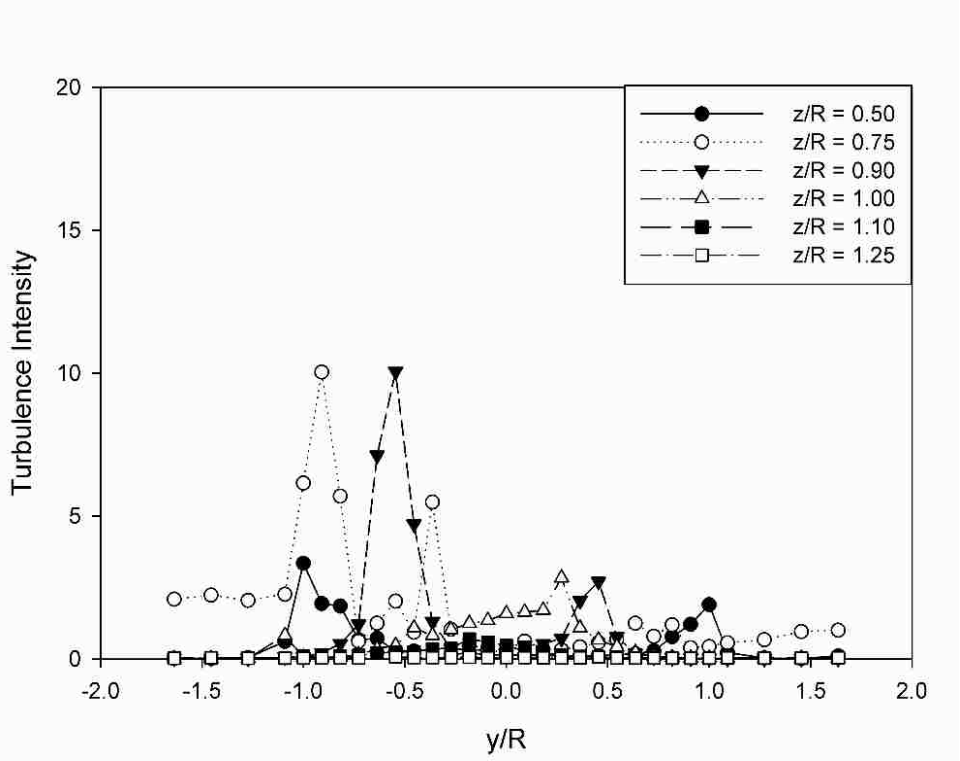

Figure 23: Turbulence Intensity at *x/R* 2.0, Yaw 10 deg.

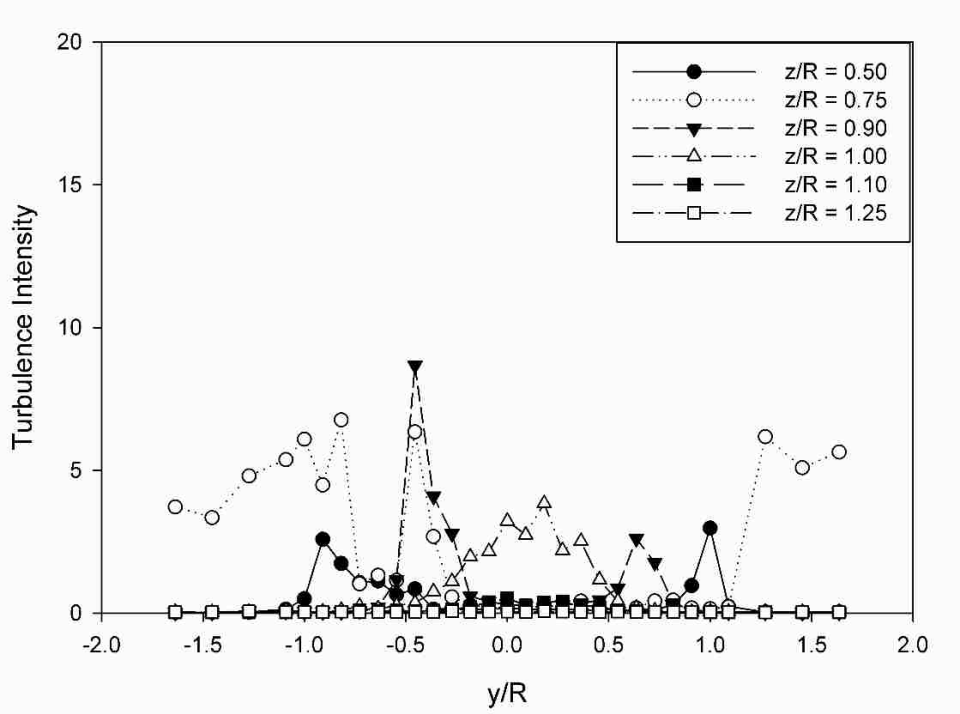

Figure 24: Turbulence Intensity at *x/R* 2.0, Yaw 15 deg.

By observing the steady state case of 0-degrees yaw, it is clear the relatively large turbulence intensities occur in the *z/R* 0.5 to ~0.75 range as the magnitude seems to quickly drop off once a large radial distance from the turbine is reached. It is also observed that the peaks in turbulence intensity occur between *y/R* equal to 0.5 and 1.0. The peaks in the 1.0 region would seem to be represented by tip vortices from the rotor. The increase in turbulence intensity in that inner region it would also be presumed to be a result of some sort of shedding from the turbine rotor.

At a yaw angle of 10 degrees, there is a marked decrease in the turbulence intensity at one radial distance on both sides of the wake profile at the radial distance at a *z/R* of 0.75. This coincides with a marked increase in the turbulence intensity at a *z/R* of 0.90. The magnitude of the turbulence intensity is approximately the same for both radial distances. However, there is a

noticeable movement in the negative direction in the profiles peak. This trend can additionally be seen in the *z/R* of 0.50 profile. The turbulence intensity peak appears to move closer to the centerline of the velocity profile with increasing radial distance, alone with being more focused on the negative portion of the profile.

At a yaw angle of 15 degrees, the same trends as the 10-degree yaw case are present. However, there are more spikes at other portion of the profile that make the trend less clear. It is the author's opinion that some of the trends in the center line portion of the velocity profile, in the -0.25 to +0.25 regions may be affected by the turbine body. What remains clear is that with an increased yaw angle the turbulence intensity spikes appear to trend closer to the centerline of the velocity profile. The extended turbulence intensities of the *z/R* 0.75 wake profile would appear to indicate that the turbulence intensity appears to be focused on this radial location.

Characterization at Different Downstream Locations

The below plots characterize the turbulence intensity profiles at varying *x/R* downstream location at a radial *z/R* distance of 0.75 and a constant yaw angle for each plot.

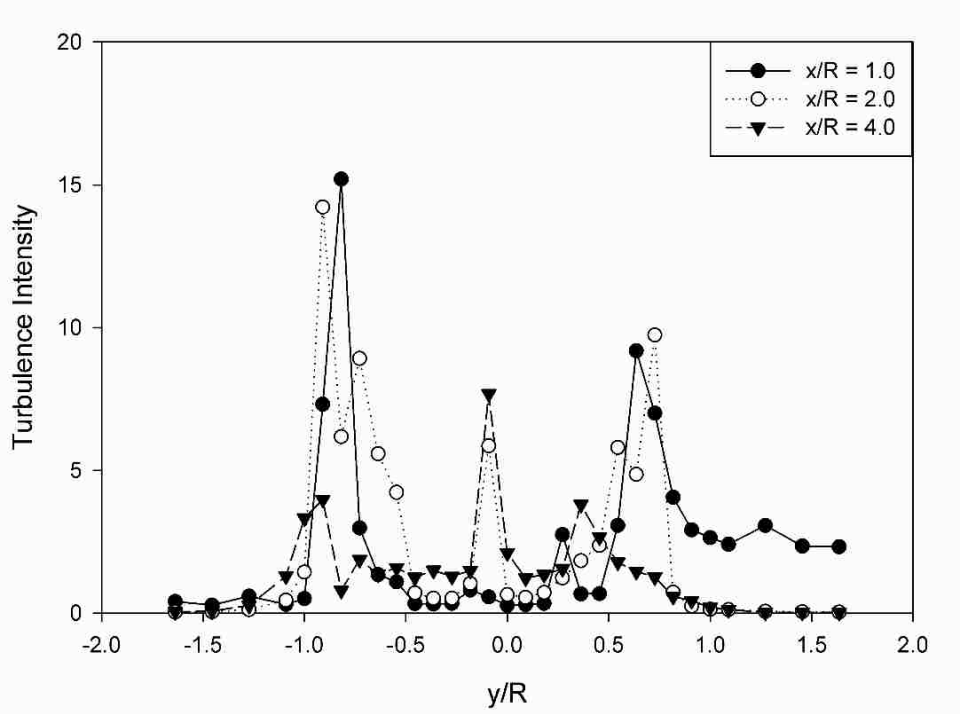

Figure 25: Turbulence Intensity at *z/R* 0.75, Yaw 0 deg.

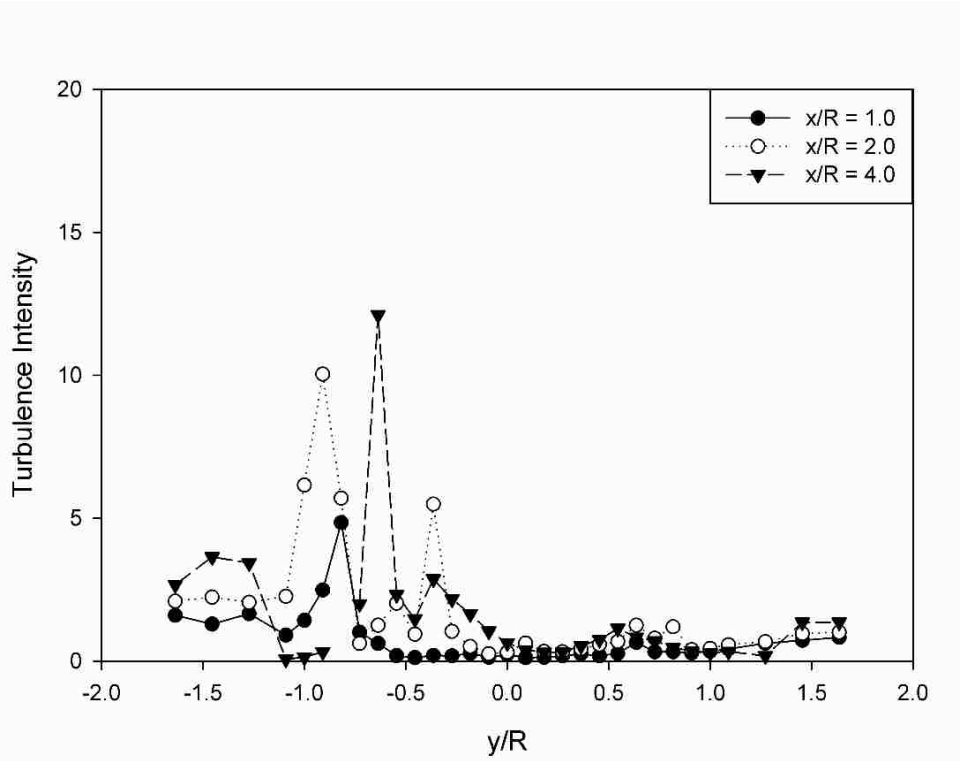

Figure 26: Turbulence Intensity at *z/R* 0.75, Yaw 10 deg.

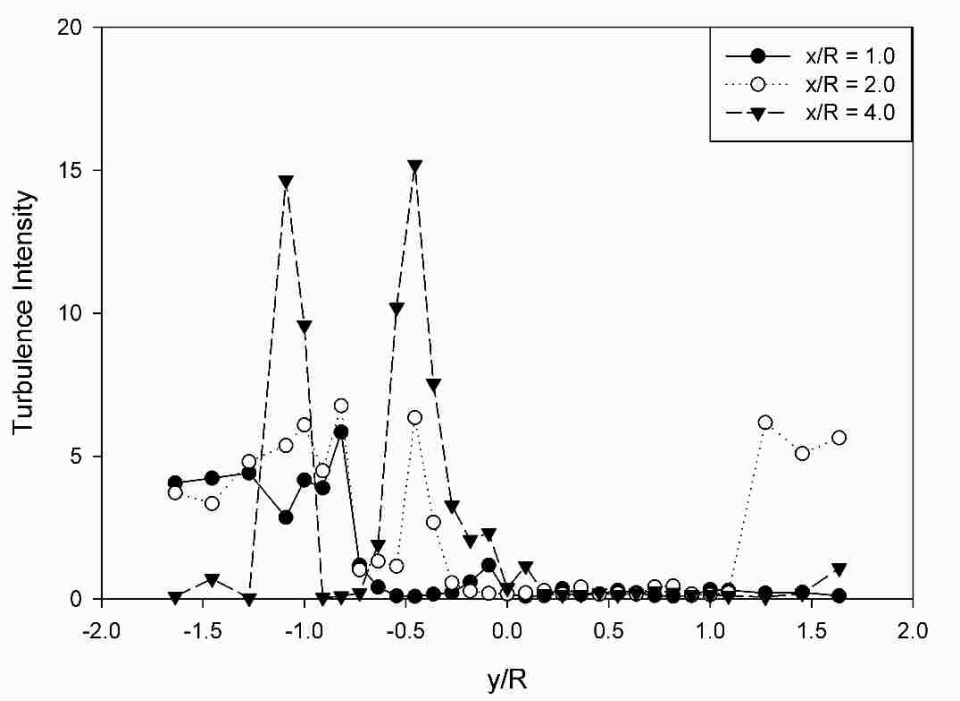

Figure 27: Turbulence Intensity at *z/R* 0.75, Yaw 15 deg.

In the baseline case of 0-degree yaw, the turbulence intensity profile is approximately symmetric. There are two symmetric peaks in turbulence intensity at approximately 1.0 *y/R* on either side of the velocity profile as well as a peak in the center. The symmetric peaks are presumably a result of vortices being shed from the tip of the rotor of the turbine. The peak at the center of the profile is due to the rotating shaft imparting energy into the flow. A symmetric turbulence intensity profile is the expected result for a 0-degree yaw case. It can additionally be observed that at a downstream location of *x/R* 4.0 the magnitude has decreased, but the same trends across the profile remain. Presumably, this is due to the profile returning to a less turbulent flow as the downstream distance increases; the flow is returning to being a more uniform flow closer to the U_∞ velocity profile.

As the yaw angles increase the one sidedness of the turbulence intensity spikes become more evident. At a yaw angle of 10 and 15 degrees the spikes on the positive side of the turbine's velocity profile all but disappear. In addition, there is a visible trend of the turbulence intensity increasing with increasing downstream distance. A dual peak in turbulence intensity on the negative portion of the velocity profile additionally becomes noticeable. It is possible that the second spike is due to the shaft. However, the increasing intensity is unexplained. At higher yaw angles, there are noticeable peaks in turbulence intensity at *y/R* value at both 0.5 and 1.0. The magnitudes of the twin spikes are additionally increasing with increasing downstream distance.

There is a noticeable movement of the location of the spikes centered around 1.0 and 0.5 *y/R*, however, from the current data, it is not possible to observe a discernable trend related to either yaw angle or downstream distance in the movement in those peaks. A particularly interesting trend is that with increasing yaw angle is the reversal of the trend of turbulence intensities at a 0-degree yaw angle. The base line case a 0-degrees yaw shows decreasing turbulence intensities with increasing downstream distance. However, as the yaw angle increases, the trend reverses, and an increase in turbulence intensity is seen with increasing downstream distance.

4.3. Swirl

The below plots illustrate the swirl number calculated at an *x/R* distance of 1.0 taken at a 0-degree yaw angle. The intent of this experimental run was to both characterize the swirl number for the flow by creating a base line case, as well as having a basic experimental case for various yaw angles.

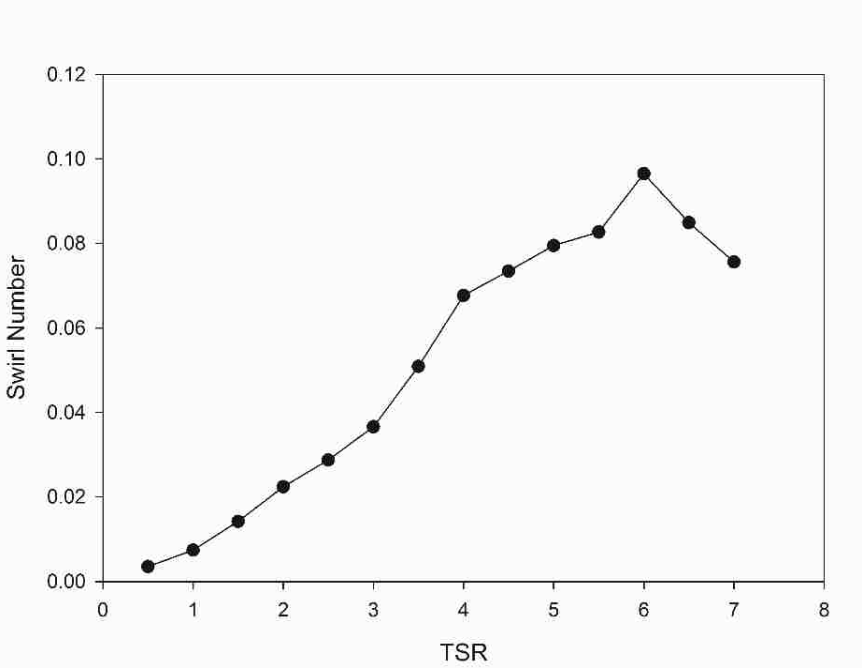

Figure 28: Experimental Swirl Number at *x/R* of 1.0, Yaw 0 deg.

The swirl number follows a trend that we expect to see, the swirl number peaks at approximately a *TSR* of 6 and a value of .10. This swirl number is considered quite low for flow, and it represented very minimal amounts of the swirl.

Effect of Yaw Angle

Below is a comparison of the swirl number at different yaw angles at an *x/R* of 2.0. The difference that is immediately noticeably in the experimental data is that as the downstream distances increase, the peak in swirl number is additionally moved to a lower *TSR*. In addition, there is a noticeable second peak that emerges at higher *TSRs*. The second peak is most noticeable at a yaw angle of 0. However, there are interesting fluctuations at higher angles of yaw that do not qualify as a second peak. The trend that presents itself is that as the yaw angle increases so does the swirl number independent of *TSR*. The distinct shape of the Swirl Number versus *TSR* curve

as the yaw angle increases becomes increasingly muddled. This ‘muddle’ the author believes is a result of the increasing turbulent nature of the flow around a high yaw angle turbine, thus why a clear curve is no longer present.

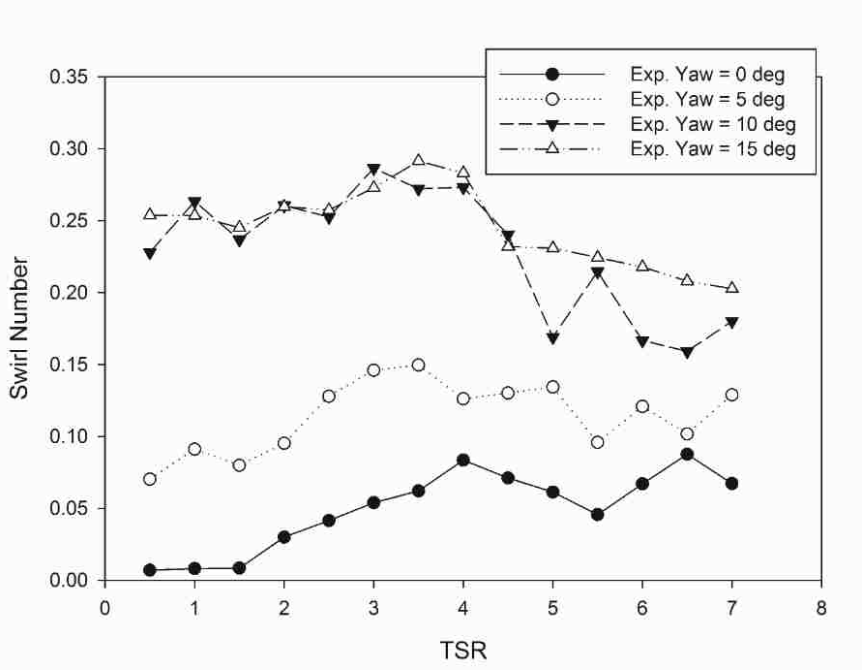

Figure 29: Experimental Swirl Number at *x/R* of 2.0

5. Higher Order Flow Characteristics

5.1. Skewness

Effect of Yaw Angle

Below are plots that characterize the Skewness of *u* component velocity time trace for varying yaw angles at constant downstream and radial locations.

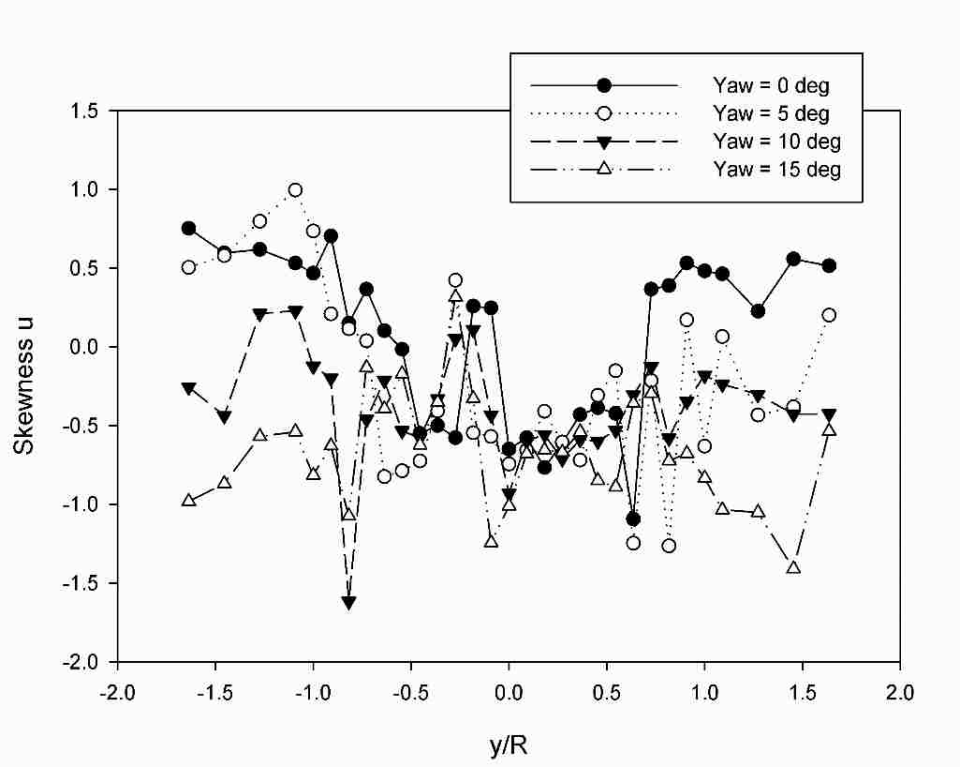

Figure 30: Skewness at x/R = 1.0, z/R = 0.75

It can be observed that the skewness tends to increase beyond one radial distance at low yaw angles. As the yaw angle increases the skewness tends to decrease beyond a radial distance of 1.0. The center of the wake profile centers on -0.5, except for center based spikes, which does not vary with yaw angle.

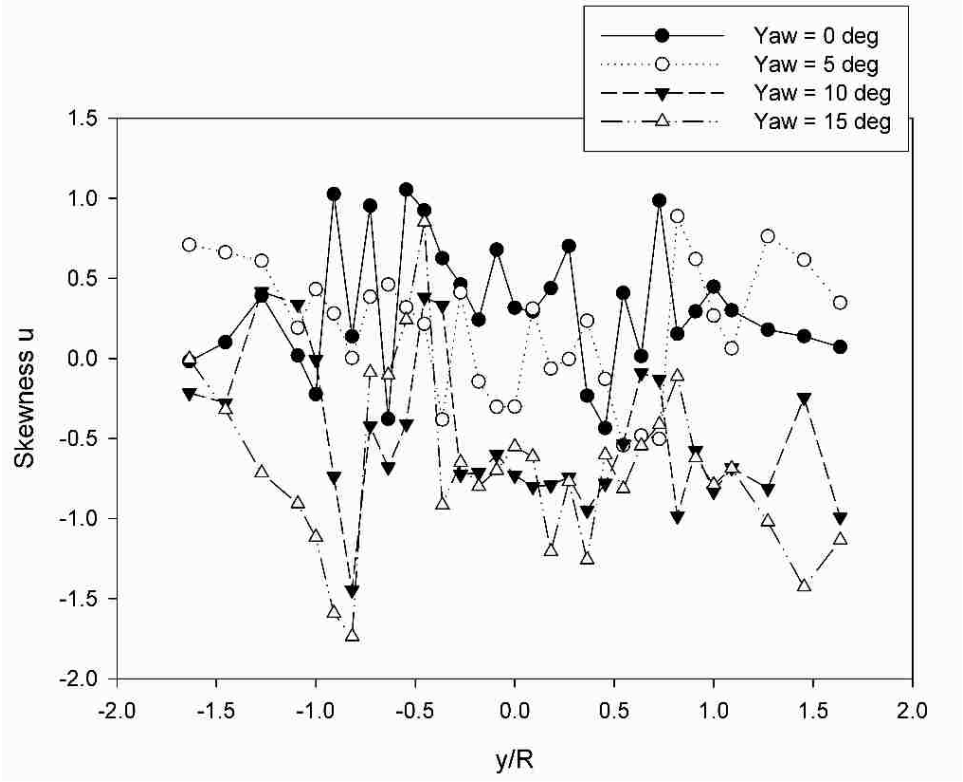

Figure 31: Skewness at x/R = 2.0, z/R = 0.75

At an increased downstream distance of x/R 2.0, there is a noticeable increase in variations of skewness at varying yaw angles. At low yaw angles of 0 and 5 degrees, the skewness tends to fall in the positive range. As the yaw angle increase, the skewness reverses in magnitude and focuses in the negative range. This indicates that with increasing yaw angle there is a heavier percentage of points that fall below the mean, a trend that reverses from lower yaw angles where the skew starts positive indicating the opposite.

Characterization at Different Radial Locations

The below plots characterize the skewness of *u* component of velocity time trace at a constant downstream distance, constant yaw angle, and varying radial distance.

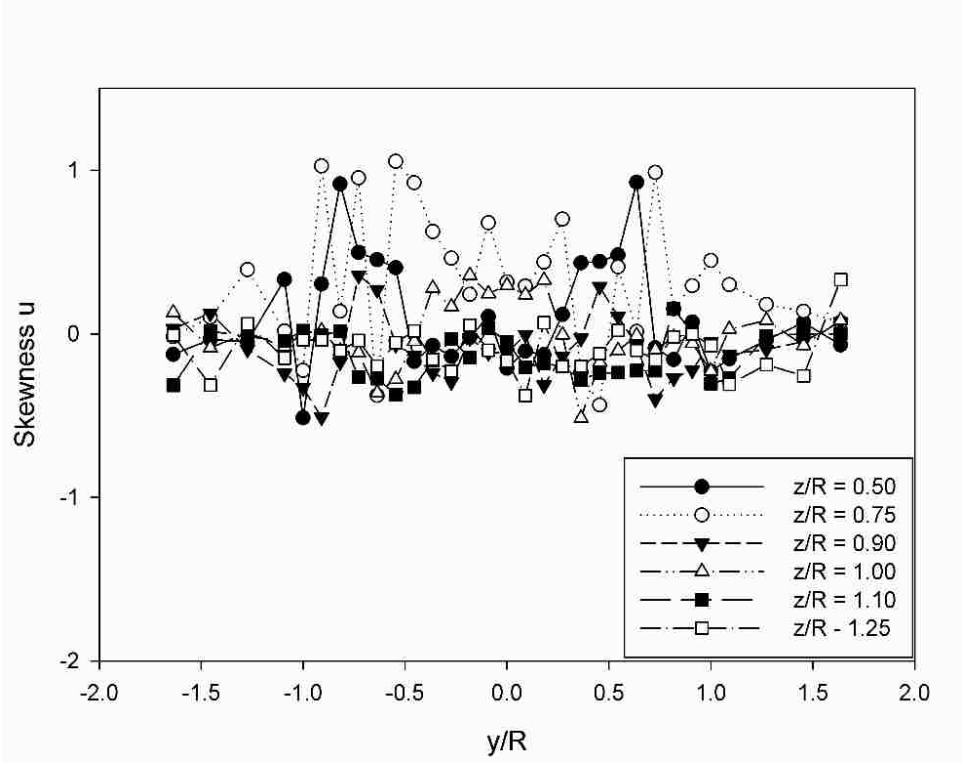

Figure 32: Skewness at *x/R* 2.0, Yaw 0 deg.

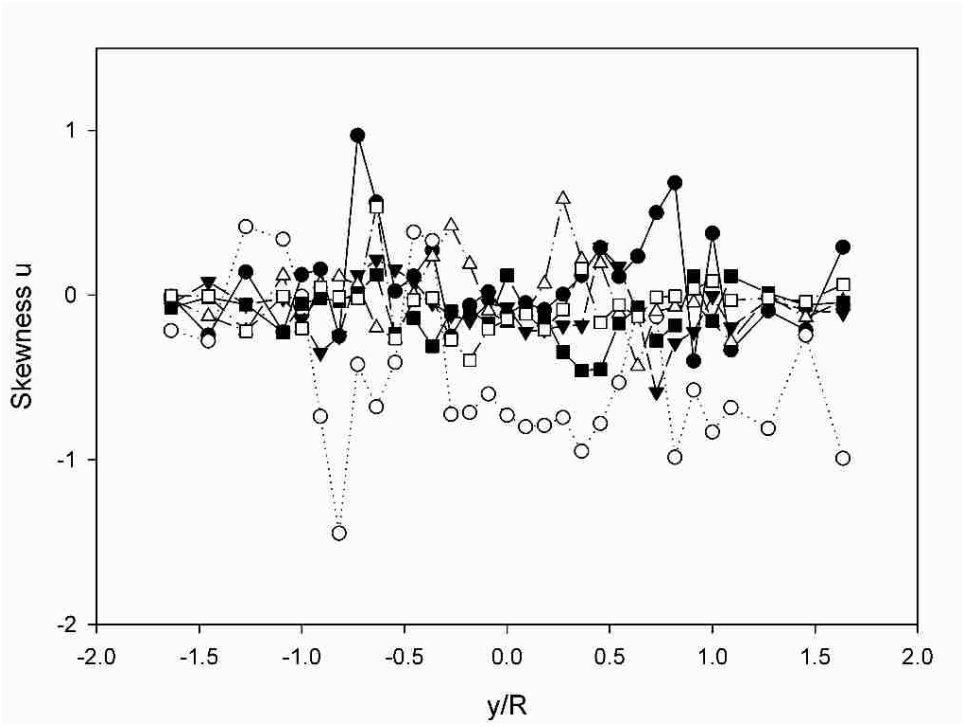

Figure 33: Skewness at *x/R* 2.0, Yaw 10 deg.

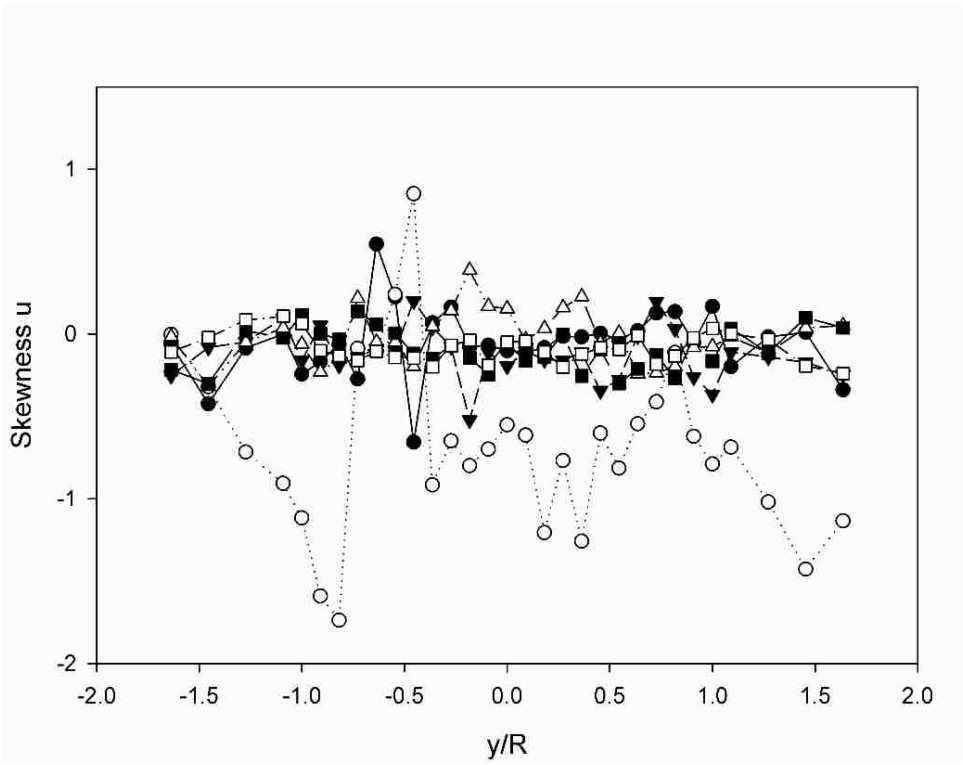

Figure 34: Skewness at *x/R* 2.0, Yaw 15 deg.

With increasing radial distance, it is quite noticeable that skewness decreases. This trend is independent of yaw angle. At radial distances of 0.50 and 0.75, there are variations across the wake profile. With increasing yaw angle the variations at those radial locations increase with increasing yaw angle. At radial locations, greater than 0.75 the skewness remains consistent at a near 0 value independent of yaw angle. This indicates that there is increasing stability in the captured velocity time traces as the ADV is moved radially up away from the turbine, independent of yaw angle.

Characterization at Different Downstream Locations

Below are plots that characterize the skewness at a constant radial location and yaw angle, and at varying downstream locations.

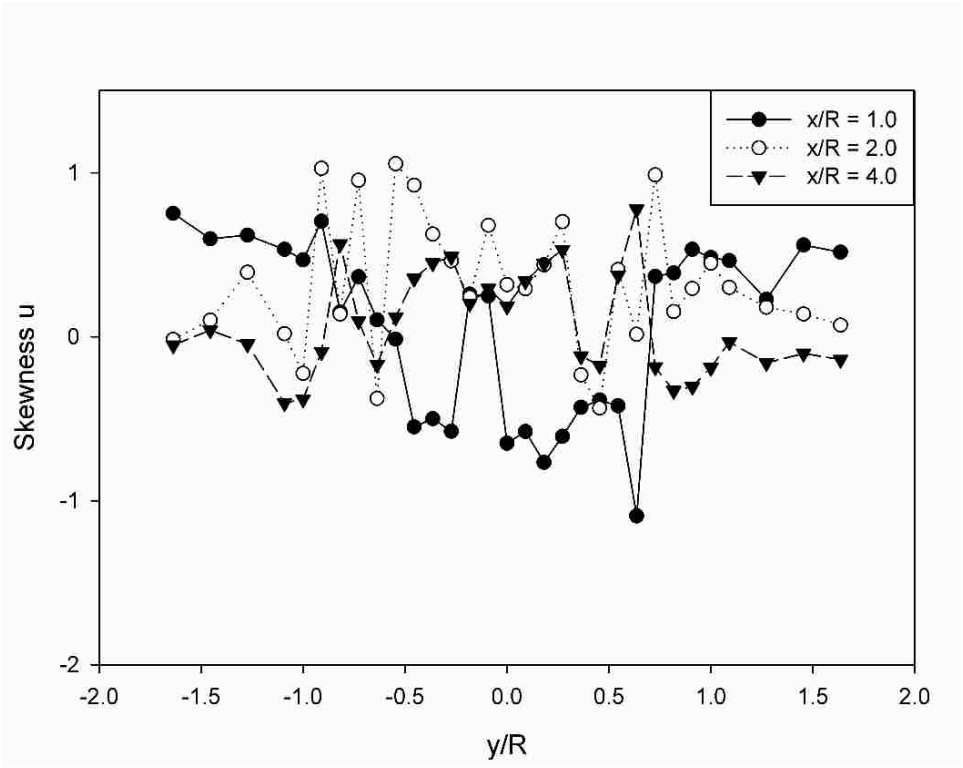

Figure 35: Skewness at *z/R* 0.75, Yaw 0 deg.

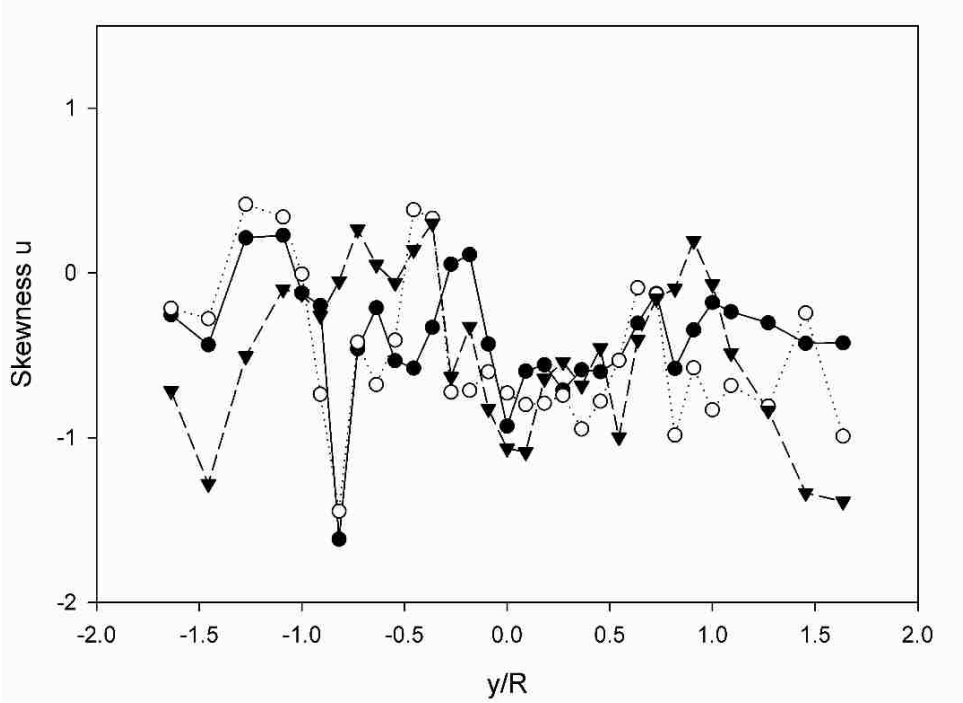

Figure 36: Skewness at *z/R* 0.75, Yaw 10 deg.

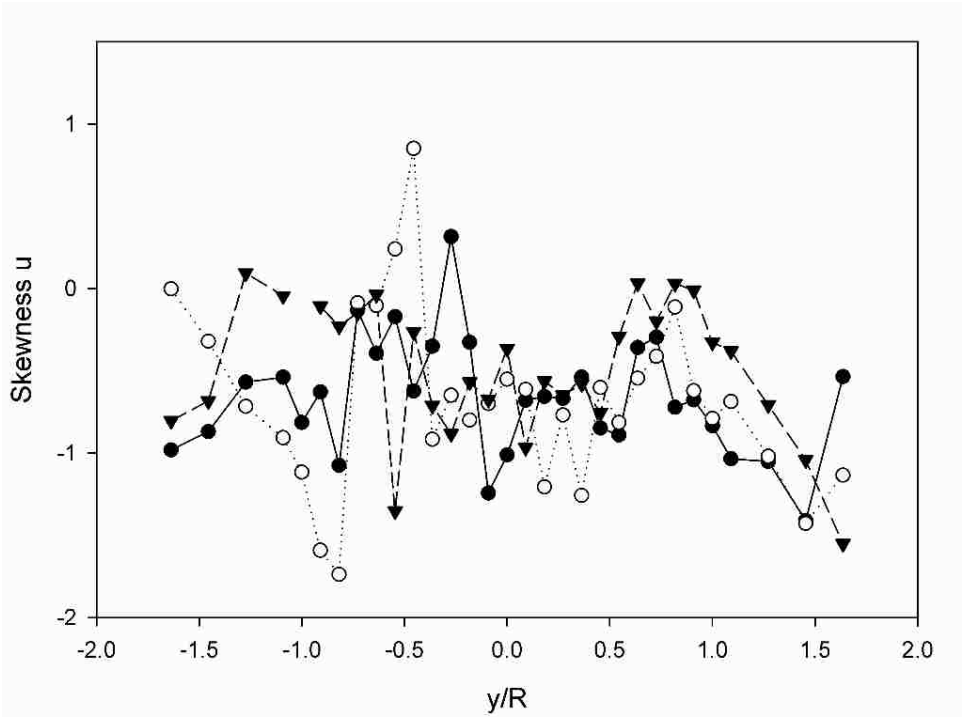

Figure 37: Skewness at *z/R* 0.75, Yaw 15 deg.

There does not appear to be a prevailing trend that presents itself with increasing downstream distance. With increasing, yaw angle skewness presents a decreasing trend. As the yaw angle increases, each time trace captures more of a left-hand tail focused a portion of the velocity distribution. This would tend to indicate that with increasing yaw angle there are more low value velocities captured in each time trace.

5.2. Kurtosis

Effect of Yaw Angle

The below plots characterize the kurtosis of *u* velocity time trace at a constant downstream distance, radial location, and at varying yaw angles.

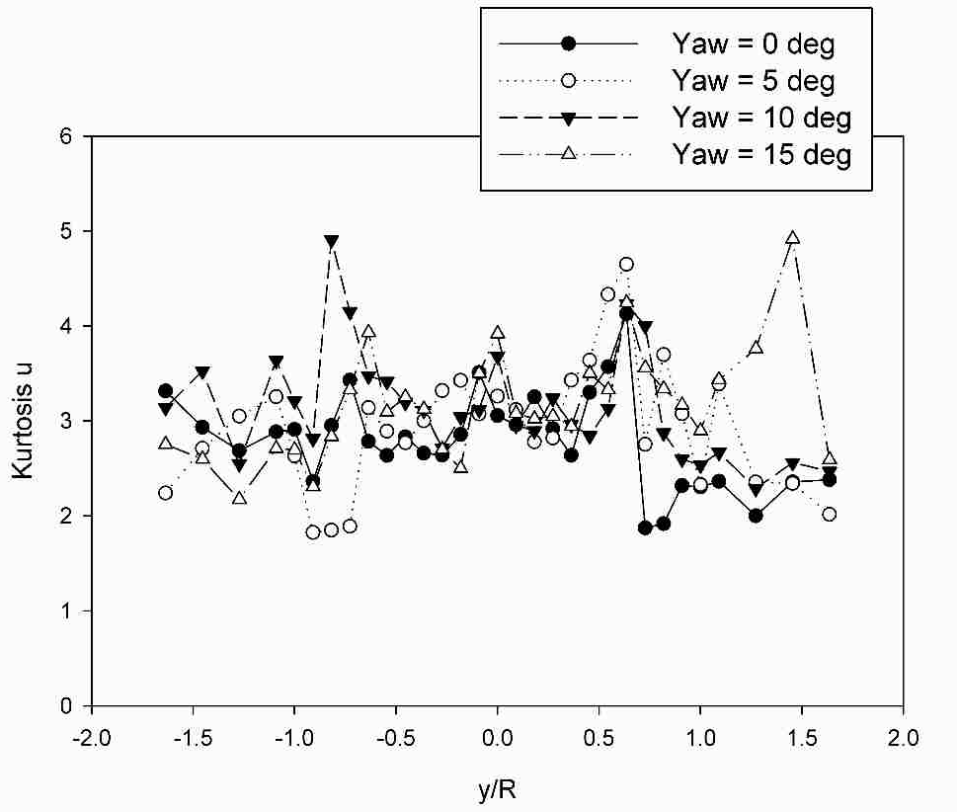

Figure 38: Kurtosis at $x/R = 1.0$, $z/R = 0.75$

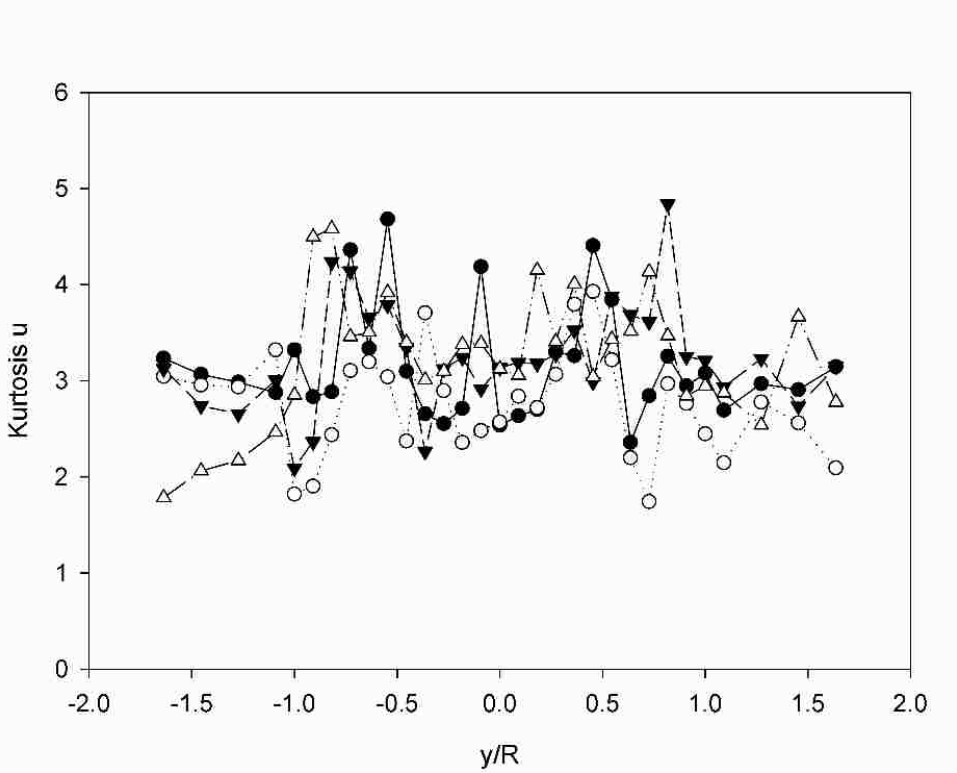

Figure 39: Kurtosis at $x/R = 2.0$, $z/R = 0.75$

Each plot for is centered around a kurtosis value of 3 which indicates that the data sets are approximate as outlier prone as a normal distribution. Increases in kurtosis are focused primarily at y/R locations of 1.0 and in the near wall regions. The increase in turbulence intensity occurring at the y/R locations of approximately 1.0 coincide with the regions where there are spikes in kurtosis. The occurrence of both these spikes in the same region makes sense because from a qualitative level they both represent an increase in the turbulent nature of the flow presumably from the shedding of tip vortices.

Characterization at Different Radial Locations

The below plots characterize the kurtosis of *u* velocity time trace at a constant downstream distance, constant yaw angle, and varying radial location.

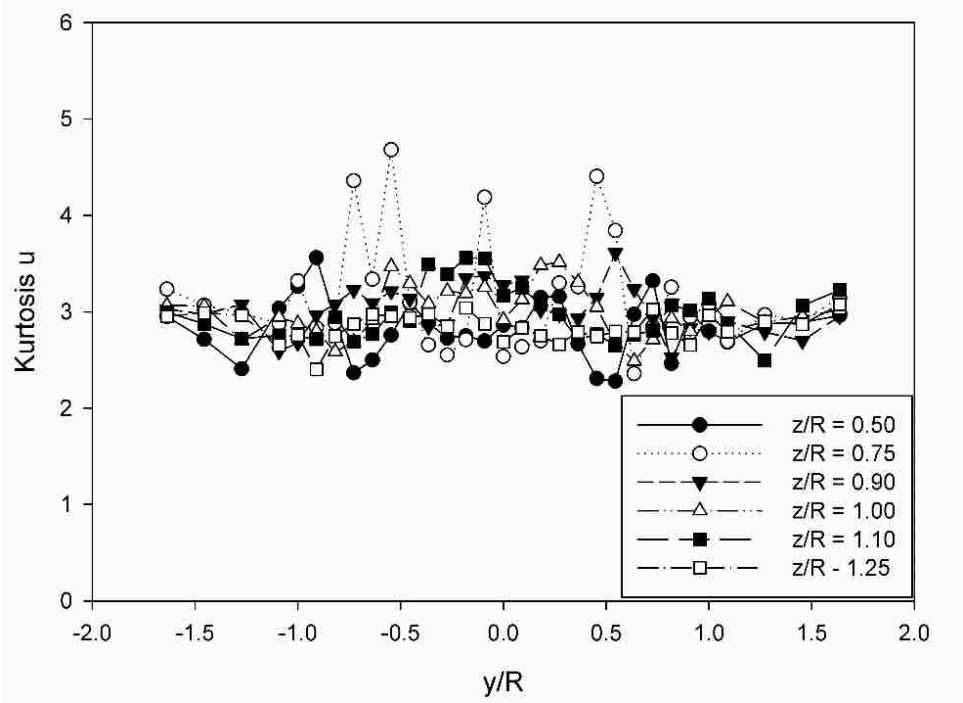

Figure 40: Kurtosis at *x/R* 2.0, Yaw 0 deg.

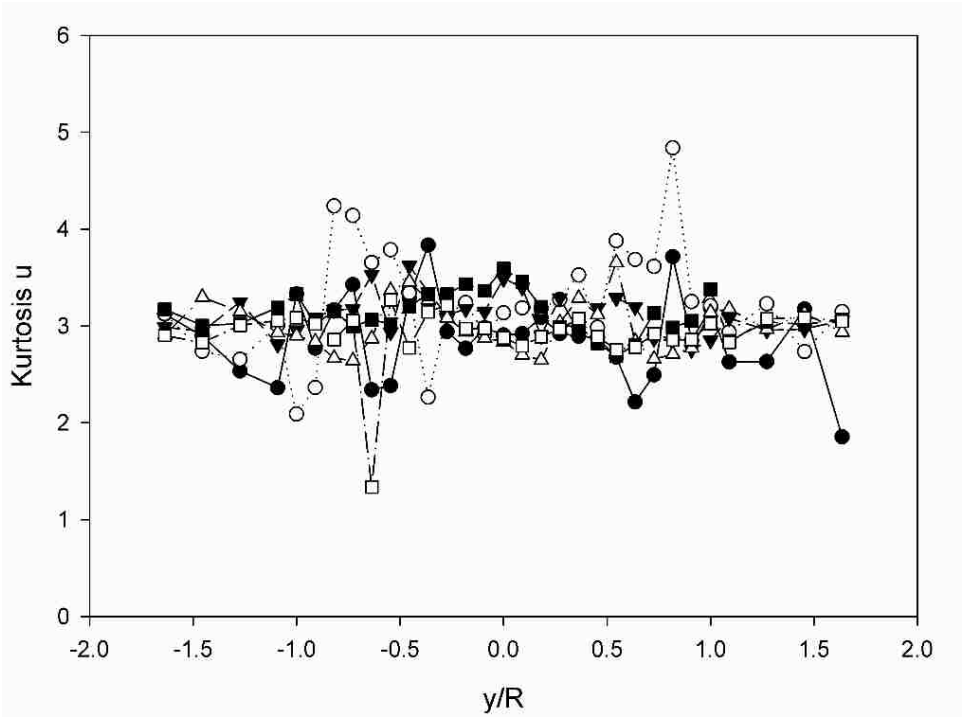

Figure 41: Kurtosis at *x/R* 2.0, Yaw 10 deg.

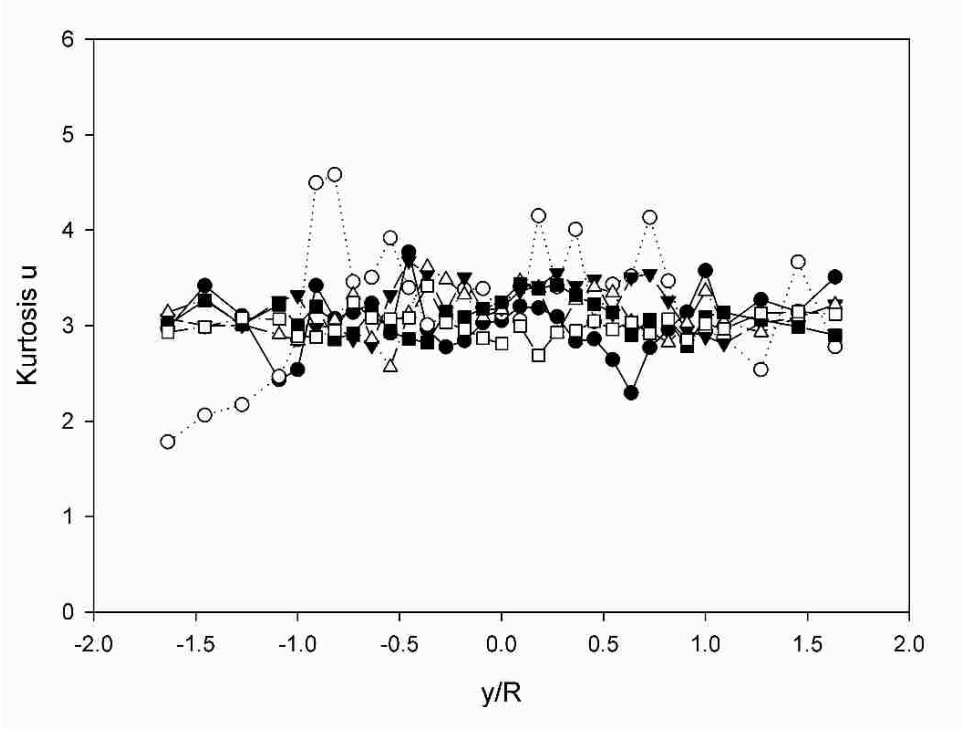

Figure 42: Kurtosis at *x/R* 2.0, Yaw 15 deg.

Each of these datasets is firmly centered around 3.0, which is to be expected for a velocity time trace that follows a distribution similar to the normal distribution. It is additionally noticeable that spikes in kurtosis tend to only occur in the radial locations closer to the turbine. At *z/R* location of 0.50 and 0.75, there are noticeable spikes in kurtosis. However no clear trend in *y/R* location presented itself to indicate where the spikes are coming from. There does not appear to be any trend correlated with change in yaw angle.

Characterization at Different Downstream Locations

The below plots characterize the kurtosis of u velocity time trace at a constant radial location, constant yaw angle, and varying downstream location.

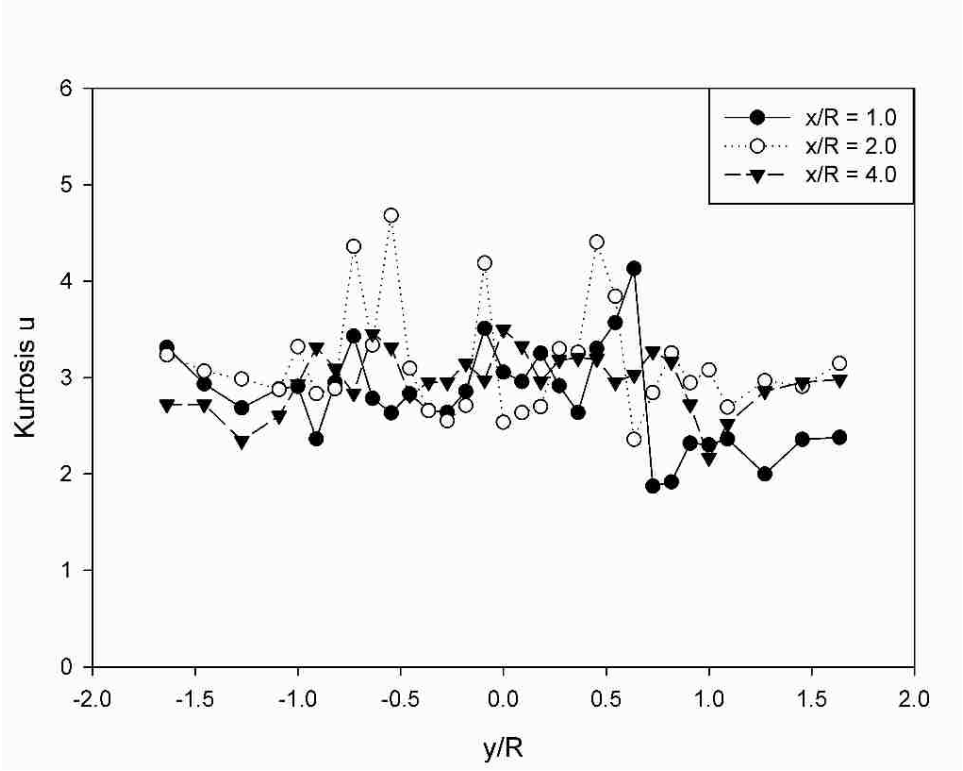

Figure 43: Kurtosis at *z/R* 0.75, Yaw 0 deg.

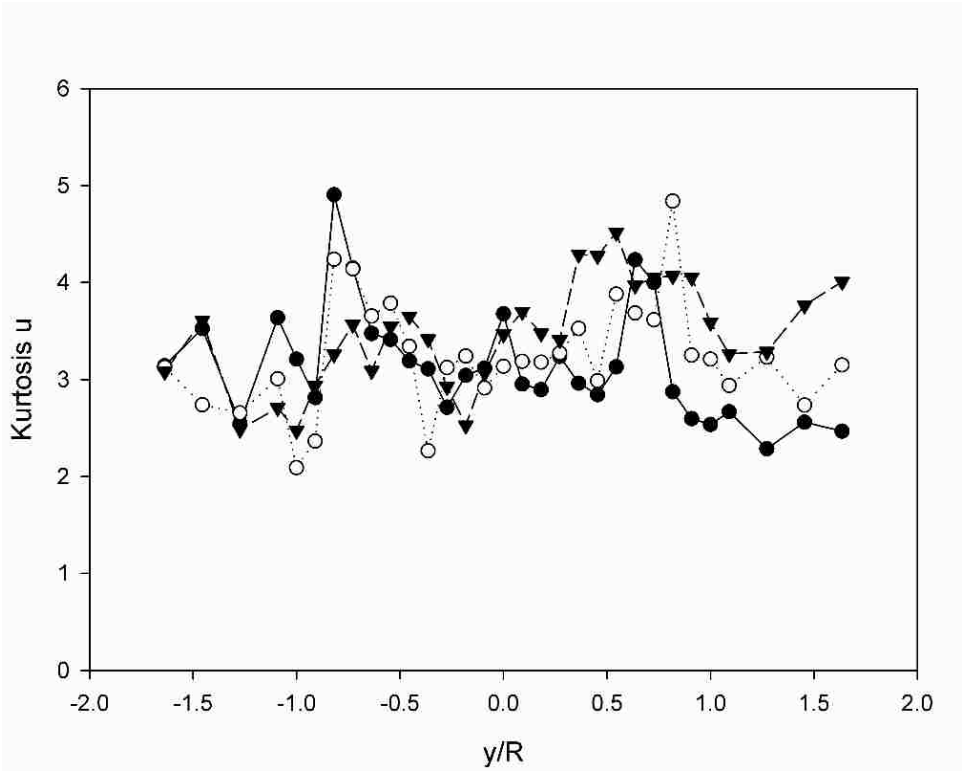

Figure 44: Kurtosis at *z/R* 0.75, Yaw 10 deg.

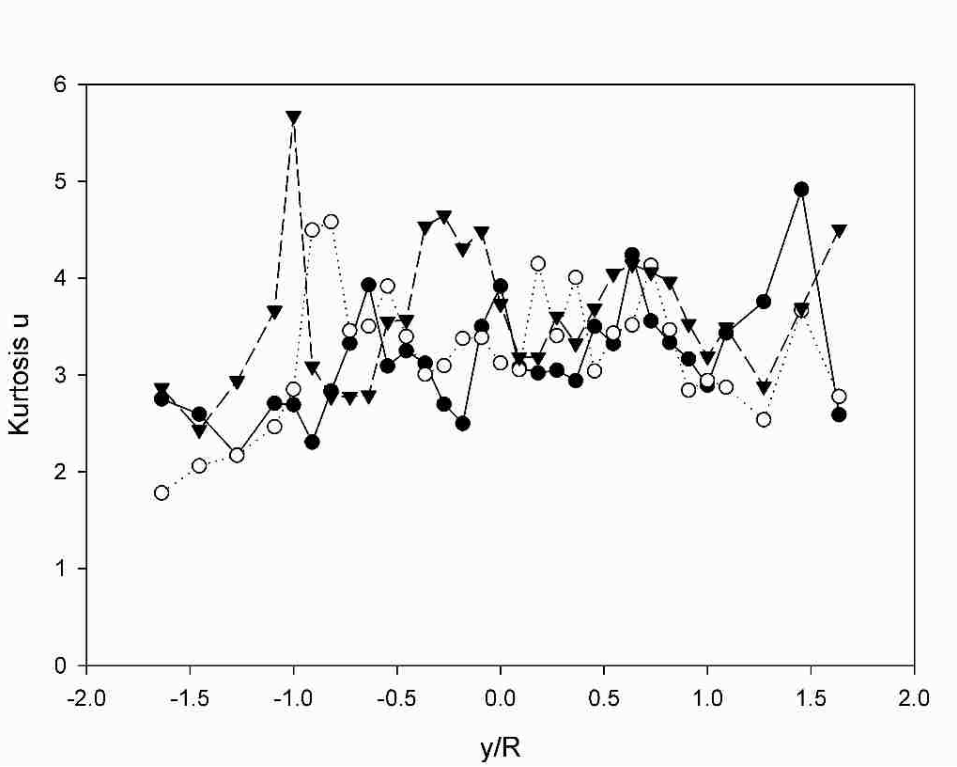

Figure 45: Kurtosis at *z/R* 0.75, Yaw 15 deg.

The kurtosis of the velocity time traces remains nominally centered around a value of 3.0 regardless of downstream distance and yaw angle. The ‘tightness’ of the varying downstream distances around 3.0 appears to spread wider as the yaw angle increases. This would indicate that with an increasing yaw angle the wake profile becomes more outlier prone than at lower yaw angles.

6. Conclusion

By analyzing mean flow characteristics, the swirl number, and higher order flow characteristics of a tidal turbine under yaw it was possible to characterize the near wake of a tidal turbine under yaw. Through looking at multiple radial locations, it was additionally possible to analyze the profile of the wake at various yaw angles. By additionally analyzing multiple downstream distances as well it is possible to look at how those wake profiles evolve as the wake propagates downstream. One of the conclusions that can be draw from the u^* results is that the 'spread' of the wake, shown by the increasing right hand side y/R velocity deficit, increases with increasing yaw angle. In addition, the top of wake is seen at a z/R of approximately 1.10, which is independent of yaw angle. Regarding turbulence intensity, it can be concluded that the largest turbulence intensities are seen in the z/R 0.50 – 0.75 radial range, and in the y/R 0.50 – 1.0 range. It can also be concluded that the swirl number of the flow increases with increasing yaw angle, independently of increasing TSR. The conclusion that skewness and kurtosis are primarily only variant and noticeable in the radial z/R range of 0.50-0.75 can also be drawn.

7. References

[1] M.J. Beam, B.L. Kline, B.E. Elbing, W. Straka, A.A. Fontaine, M. Lawson, Y. Li, R. Thresher, M. Previsic, Marine Hydrokinetic Turbine Power-Take-Off Design for Optimal Performance and Low Impact on Cost-of-Energy, ASME 2013 32nd International Conference on Ocean, Offshore and Arctic Engineering, American Society of Mechanical Engineers, 2013, pp. V008T009A041-V008T009A041.

[2] R. Uria-Martinez, P. W. O'Connor, M. M. Johnson, 2014 Hydropower Market Report, U.S Department of Energy, 2015, pp. 1-100.

[3] D. Magagna, A. Uihlein, Ocean energy development in Europe: Current status and future perspectives, International Journal of Marine Energy, 11 (2015) 84-104.

[4] N.D. Laws, B.P. Epps, Hydrokinetic energy conversion: Technology, research, and outlook, Renewable and Sustainable Energy Reviews, 57 (2016) 1245-1259.

[5] P.W. Carlin, A.S. Laxson, E. Muljadi, The history and state of the art of variable-speed wind turbine technology, Wind Energy, 6 (2003) 129-159.

[6] A. Swift, J. Firmer, An Investigation of Sidewheel Yaw Control for Horizontal Axis Wind Turbines, Fifth ASME Wind Energy Symposium: presented at the Ninth Annual Energy-Sources Technology Conference and Exhibition, New Orleans, Louisiana, February 23-27, 1986, American Society of Mechanical Engineers, 1986, pp. 47.

[7] T. Friis Pedersen, S. Gjerding, P. Enevoldsen, J. Hansen, H. Jørgensen, Wind turbine power performance verification in complex terrain and wind farms, Risø National Laboratory, Roskilde, 2002.

[8] P.Å. Krogstad, M.S. Adaramola, Performance and near wake measurements of a model horizontal axis wind turbine, Wind Energy, 15 (2012) 743-756.

[9] D. Medici, P. Alfredsson, Measurements on a wind turbine wake: 3D effects and bluff body vortex shedding, Wind Energy, 9 (2006) 219-236.

[10] Á. Jiménez, A. Crespo, E. Migoya, Application of a LES technique to characterize the wake deflection of a wind turbine in yaw, Wind Energy, 13 (2010) 559-572.

[11] P. Parkin, R. Holm, D. Medici, The application of PIV to the wake of a wind turbine in yaw, Particle Image Velocimetry; Gottingen; 17 September 2001 through 19 September 2001, 2001, pp. 155-162.

[12] M.F. Howland, J. Bossuyt, L.A. Martinez-Tossas, J. Meyers, C. Meneveau, Wake Structure of Wind Turbines in Yaw under Uniform Inflow Conditions, arXiv preprint arXiv:1603.06632, 2016.
[13] J.J. Trujillo, F. Bingöl, G.C. Larsen, J. Mann, M. Kühn, Light detection and ranging measurements of wake dynamics. Part II: two-dimensional scanning, Wind Energy, 14 (2011) 61-75.
[14] P.K. Modali, N. Kolekar, Performance and Wake Characteristics of a Tidal Turbine under Yaw, in: A. Banerjee (Ed.), 2017.
[15] P. Galloway, Performance quantification of tidal turbines subjected to dynamic loading, University of Southampton, 2013.
[16] S. Park, S. Park, S.H. Rhee, Influence of blade deformation and yawed inflow on performance of a horizontal axis tidal stream turbine, Renewable Energy, 2014, pp. 321-332.
[17] N. Kolekar, A. Banerjee, Performance characterization and placement of a marine hydrokinetic turbine in a tidal channel under boundary proximity and blockage effects, Applied Energy, 148 (2015) 121-133.
[18] Datasheet Vectrino Lab, Nortek AS, 2017.
[19] C.E. Morris, D.M. O'Doherty, A. Mason-Jones, T. O'Doherty, Evaluation of the swirl characteristics of a tidal stream turbine wake, International Journal of Marine Energy, 14 (2016) 198-214.
[20] P. Modali, On Performance and Wake Characteristics of a Tidal Turbine under Yaw, 2016.